



Critical metals in manganese nodules from the Cook Islands EEZ, abundances and distributions

James R. Hein ^{a,*}, Francesca Spinardi ^a, Nobuyuki Okamoto ^b, Kira Mizell ^a, Darryl Thorburn ^c, Akuila Tawake ^d

^a U.S. Geological Survey, PCMSC, 400 Natural Bridges Dr., Santa Cruz, CA 95060, USA

^b Sea-Floor Mineral Resources R&D Division, Metals Mining Technology Dept., JOGMEC, 2-10-1 Toranomon, Minato-ku, Tokyo 105-0001, Japan

^c Seabed Minerals Authority, Avarua, Rarotonga, Cook Islands

^d SOPAC Division of the SPC, Private Mail Bag, GPO, Suva, Fiji



ARTICLE INFO

Article history:

Received 20 August 2014

Received in revised form 8 December 2014

Accepted 12 December 2014

Available online 8 January 2015

Keywords:

Manganese nodules

Cook Islands EEZ

Critical metals

Mn

Ti

Co

Ni

REY

ABSTRACT

The Cook Islands (CIs) Exclusive Economic Zone (EEZ) encompasses 1,977,000 km² and includes the Penrhyn and Samoa basins abyssal plains where manganese nodules flourish due to the availability of prolific nucleus material, slow sedimentation rates, and strong bottom currents. A group of CIs nodules was analyzed for mineralogical and chemical composition, which include many critical metals not before analyzed for CIs nodules. These nodules have varying sizes and nuclei material; however all are composed predominantly of δ-MnO₂ and X-ray amorphous iron oxyhydroxide. The mineralogy, Fe/Mn ratios, rare earth element contents, and slow growth rates (mean 1.9 mm/10⁶ years) reflect formation primarily by hydrogenetic precipitation. The paucity of diagenetic input can be explained by low primary productivity at the surface and resultant low organic matter content in seafloor sediment, producing oxic seafloor and sub-seafloor environments. The nodules contain high mean contents of Co (0.41%), Ni (0.38%), Ti (1.20%), and total rare earth elements plus yttrium (REY; 0.167%), and also high contents of Mo, Nb, V, W, and Zr.

Compiled data from a series of four cruises by the Japan International Cooperation Agency and the Mining agency of Japan from 1985 to 2000 were used to generate a map that defines the statistical distribution of nodule abundance throughout the EEZ, except the Manihiki Plateau. The abundance distribution map shows a belt of high nodule abundance (19–45 kg/m²) that starts in the southeast corner of the EEZ, runs northwest, and also bifurcates into a SW trending branch. Small, isolated areas contain abundances of nodules of up to 58 kg/m². Six ~20,000 km² areas of particularly high abundance were chosen to represent potential exploration areas, and maps for metal concentration were generated to visualize metal distribution and to extrapolate estimated metal tonnages within the six sites and the EEZ as a whole. Grades for Mn, Cu, and Ni are low in CIs nodules in areas of high abundance; however, Ti, Co, and REY show high contents where nodule abundances are high. Of the six areas identified to represent a range of metal contents, one at the northern end of the N-S abundance main belt optimizes the most metals and would yield the highest dry metric tons for Mn (61,002,292), Ni (1,247,834), Mo (186,166), V (356,247), W (30,215), and Zr (195,323). When compared with the Clarion-Clipperton Zone, the CIs nodules show higher nodule abundances (>25 kg/m² over ~123,844 km²), and are more enriched in the green-tech, high-tech, and energy metals Co, Ti, Te, Nb, REY, Pt, and Zr. The CIs EEZ shows a significant resource potential for these critical metals due to their high prices, high demand, and the high nodule abundance, which will allow for a smaller footprint for a 20-year mine site and therefore smaller environmental impact.

Published by Elsevier B.V.

1. Introduction

The Cook Islands (CIs), located in the central South Pacific, consist of a northern group of six atolls and a southern group of nine islands.

Those 15 islands have a total land area of 240 km², whereas the 200 nm (360 km) Exclusive Economic Zone (EEZ) of the CIs totals 1,977,000 km², making the CIs a very large marine nation with an ocean/land ratio of 8238. The total population of Cook Islanders has varied between about 24,600 and 17,300 from 2007 to 2014, including both residents and about a quarter of the population living outside the CIs, mostly in New Zealand.

The EEZs adjacent to that of the CIs include French Polynesia to the E-SE, Kiribati to the E-NE, Tokelau to the NW, American Samoa to the west, and Niue to the SW (Fig. 1). International waters lie to the north

Abbreviations: ECS, Extended Continental Shelf; EEZ, Exclusive Economic Zone; CIs, Cook Islands; REE, Rare earth elements; REY, Rare earth elements plus yttrium

* Corresponding author.

E-mail address: jhein@usgs.gov (J.R. Hein).

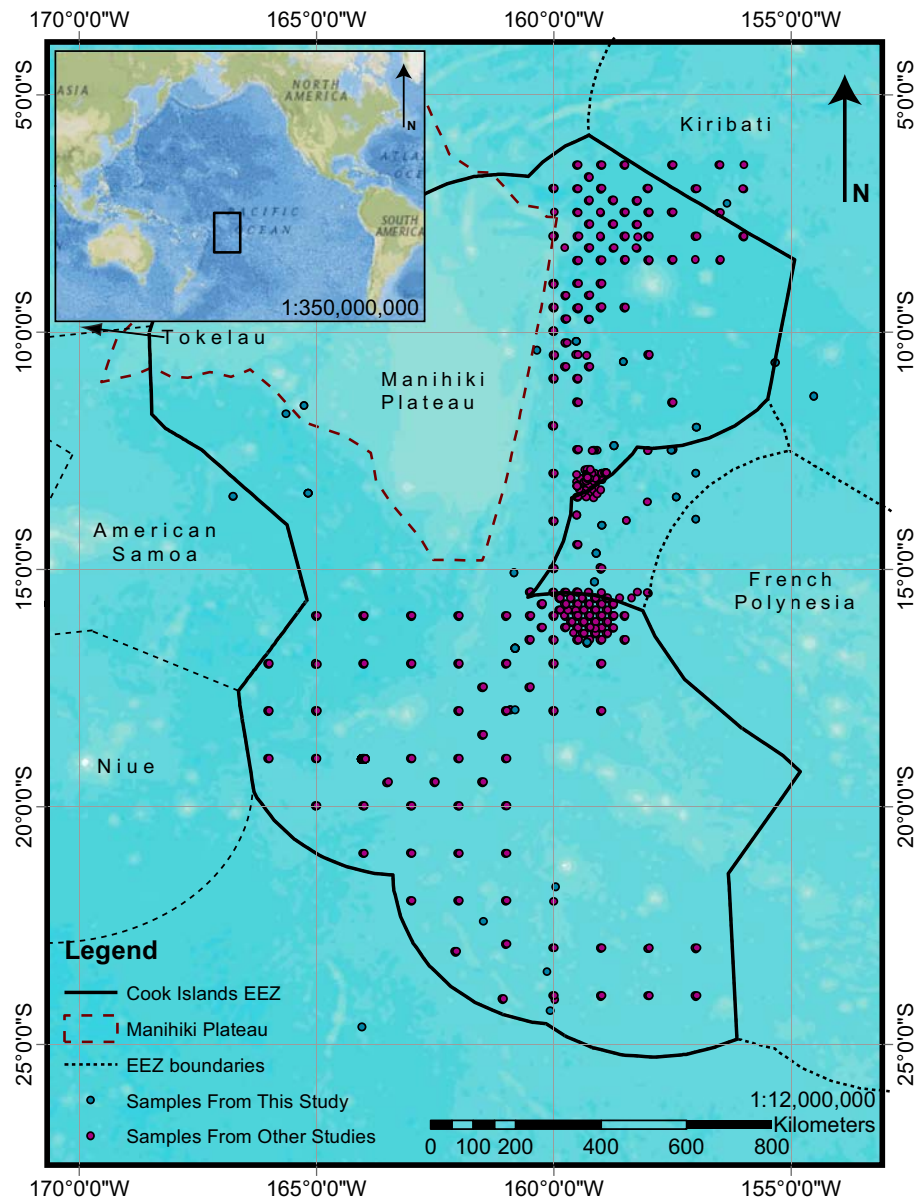


Fig. 1. Location map of the Cook Islands EEZ (inset) and a map showing sample locations analyzed for this study in blue and other samples used for this study in red from JICA/MMAJ (2001) and Okamoto (2003).

and south of the Cls EEZ and also form a “donut hole” between the EEZs of Cls, Kiribati, and French Polynesia. The Cls has a potential Extended Continental Shelf (ECS) north of the northern EEZ boundary, which is currently before the Commission on the Limits of the Continental Shelf. The physiography of the Cls EEZ consists predominantly of the Manihiki Plateau (NW quadrant) with associated small seamounts, and parts of the Penrhyn Basin and Samoa Basin abyssal plains with associated abyssal hills and small seamounts.

The abyssal seabed sediments of the Cls EEZ consist predominantly of zeolite-rich pelagic red–brown clays, but biogenic silica and carbonate increase in the sediment with decreasing latitude and at water depths of less than about 4800 m. Carbonate mud/ooze dominates in the far NE of the EEZ and in the potential ECS. The Manihiki Plateau is blanketed by calcareous and siliceous mud/ooze. The abyssal plain muds are composed of quartz, clay minerals, zeolites, volcanic glass, iron and manganese oxides, phosphate debris, and minor biogenic carbonate and silica in places (Cronan et al., 2010).

Ferromanganese nodules (hereafter Mn nodules) from the Cls EEZ are compositionally different from those in other nodule fields from the global ocean. It has been known for some time that Cls nodules have relatively high cobalt (Co) contents and low nickel (Ni), copper (Cu), and manganese (Mn) contents (e.g. Cronan et al., 1991; Verlaan et al., 2004; Hein and Petersen, 2013) compared to other nodule fields (Hein et al., 2013). The concentrations of many critical and strategic metals have not been analyzed previously for Cls nodules, so comparisons with other nodule fields have been limited. To address this, we present here chemical and mineralogical analyses for a set of nodules distributed throughout the Cls EEZ (Table 1; Appendix 1; Supplementary Table S.1) for a set of 67 elements, including all of the elements of potential economic interest, such as the rare earth elements (REEs) plus yttrium (REY), tellurium (Te), niobium (Nb), zirconium (Zr), tungsten (W), titanium (Ti), and others (Appendix 1). In addition, we recalculate the tonnages of nodules and contained metals from various nodule abundance regions (in square kilometers) determined by GIS

Table 1

Location of Cook Islands EEZ manganese nodules.

Sample number	Latitude (S)	Longitude (W)	Water depth (m)
CK-76-1 STN-03 FFC-02A	16°33.20'	159°17.50'	5089
CK-76-1 STN-03 FFG-06A	16°33.20'	159°17.50'	5093
CK-76-1 STN-03 FFG-06B	16°33.20'	159°17.50'	5093
CK-76-1 STN-04 FFC-04	15°16.00'	159°08.50'	5134
CK-76-1 STN-05 FFG-08A	14°40.00'	159°06.00'	5092
CK-76-1 STN-05 FFG-08B	14°40.00'	159°06.00'	5092
CK-76-1 STN-06 FFG-09	14°04.90'	158°59.00'	5111
CK-76-1 STN-07 FFG-10A	12°24.00'	158°44.00'	5310
CK-76-1 STN-07 FFG-10B	12°24.00'	158°44.00'	5310
CK-76-1 STN-08 FFG-11	10°38.00'	158°31.50'	5286
CK-76-1 STN-10 FFG-13	15°04.80'	160°50.00'	4999
CK-76-1 STN-11 FFG-14A	16°40.00'	160°48.50'	4793
CK-76-1 STN-11 FFG-14B	16°40.00'	160°48.50'	4793
CK-76-1 STN-11 FFG-14C-MRT-B0-7	16°40.00'	160°48.50'	4793
CK-76-1 STN-11 FFG-14C-MRU-B0-13	16°40.00'	160°48.50'	4793
CK-76-1 STN-11 FFG-14C-MRU-L0-5	16°40.00'	160°48.50'	4793
CK-76-1 STN-11 FFG-14C-MRU-L5-13	16°40.00'	160°48.50'	4793
CK-76-1 STN-11 FFG-14D	16°40.00'	160°48.50'	4793
CK-76-1 STN-12 FFG-15	17°58.00'	160°48.50'	4920
CK-78-2 STN-01 FFG-02A	13°29.20'	157°24.80'	5200
CK-78-2 STN-01 FFG-02B	13°29.20'	157°24.80'	5200
CK-78-2 STN-02 FFG-03	13°29.20'	157°24.80'	5200
CK-78-2 STN-2 FFG-03	13°29.20'	157°24.80'	5200
CK-78-2 STN-02 FFG-04	13°29.20'	157°24.80'	5200
CK-78-2 STN-03 FFG-05	12°59.20'	156°59.90'	5050
CK-78-2 STN-03 FFG-06	12°59.20'	156°59.90'	5050
CK-78-2 STN-04 FFG-07	12°30.10'	157°31.60'	5133
CK-78-2 STN-04 FFG-08	12°30.10'	157°31.60'	5133
CK-78-2 STN-05 FFG-09A	12°01.00'	156°59.50'	5275
CK-78-2 STN-05 FFG-09B	12°01.00'	156°59.50'	5275
CK-78-2 STN-05 FFG-10	12°01.00'	156°59.50'	5275
CK-78-2 STN-07 FFG-13A	13°24.00'	165°10.20'	5440
CK-78-2 STN-07 FFG-13B	13°24.00'	165°10.20'	5440
CK-78-2 STN-07 FFG-14A	13°24.00'	165°10.20'	5440
CK-78-2 STN-7 FFG-14B	13°24.00'	165°10.20'	5440
CK-78-2 STN-08 FFG-15B	13°28.70'	166°45.00'	5350
CK-78-2 STN-08 FFG-16	13°28.70'	166°45.00'	5350
CK-80-1 STN-03 WGCM-03	11°21.14'	154°31.09'	5540
CK-80-1 STN-03 WGCM-13	11°21.14'	154°31.09'	5540
CK-80-1 STN-04 WGCM4A	10°39.03'	155°20.02'	5520
CK-80-1 STN-04 WGCM-4B	10°39.03'	155°20.02'	5520
CK-80-1 STN-10 WGCM-08	07°55.54'	156°23.10'	5220
CK-80-2 STN-17 WG-01A	10°12.30'	159°31.20'	5275
CK-80-2 STN-17 WG-01B-MRT-B0-8	10°12.30'	159°31.20'	5275
CK-80-2 STN-17 WG-01B-MRU-B0-11	10°12.30'	159°31.20'	5275
1021-G991	24°38.50'	164°02.40'	5416
1021-G995	22°25.10'	161°29.00'	4715
1021-G1001	21°41.20'	159°57.10'	3970
1021-G1003	23°29.10'	160°08.40'	4817
1021-G1004	24°18.40'	160°04.50'	5070
U321A	10°23.40'	160°21.00'	5047
U339 < 20 mm	11°33.60'	165°15.00'	4219
U339 > 20 mm	11°33.60'	165°15.00'	4219
U340	11°43.80'	165°38.40'	5253

ArcMap calculations. Several assessments of contained metal tonnages for CIs EEZ nodules have been made (e.g. Clark et al., 1995; Kingan, 1998; JICA/MMAJ, 2001; Okamoto, 2003; Cronan, 2013; Hein and Petersen, 2013). Most of those assessments considered only a few metals, so here we present new estimates for the tonnages of 10 contained metals of economic interest as well as for total REY.

2. Samples and methods

Fifty-four samples and subsamples were analyzed from 27 sites. Each sample was dried and ground to a $<75\text{ }\mu\text{m}$ powder in an agate mortar and pestle. The nodule nucleus was included in the bulk analysis of each nodule sample. Element concentrations were determined by several methods. The 10 major elements (Fe, Mn, Si, Al, Mg, K, Ca, Na,

P, Ti) were analyzed using X-ray fluorescence spectroscopy on a borate-fused disc; 32 minor elements were determined by either 4-acid digest followed by induction coupled plasma-atomic emission spectroscopy (ICP-AES) and ICP-mass spectrometry (ICP-MS; Ag, As, Ba, Be, Bi, Cd, Co, Cr, Cu, Ga, In, Li, Pb, Rb, S, Sb, Sc, Sn, Sr, Ta, Th, Tl, Zn), or lithium metaborate fusion and ICP-MS (Cs, Hf, Mo, Nb, Ni, U, V, W, Zr, REY); platinum-group elements and gold were determined by Ni-fire assay and ICP-MS, Cl by specific-ion electrode, Hg by cold vapor analysis, H_2O^- by gravimetric analysis, and H_2O^+ by penfield-infrared. Se and Te were determined by 4-acid digestion hydride generation with a modified flow injection technique developed for high Mn samples and analyzed using atomic absorption spectroscopy. Duplicate analyses were performed on 30% of the samples and the average precision was approximately $\pm 3\%$ for all techniques.

Mineral composition was determined using a Philips X-ray diffractometer (XRD) with $\text{CuK}\alpha$ radiation and graphite monochromator run from 4° to $71^\circ 20'$ at 40 kV and 45 mA. Digital scan results were analyzed using Philips X'pert High Score software to measure X-ray reflections and identify possible mineral compositions. The identification of minerals was constrained using the chemical composition.

Pearson product correlation coefficient matrices were calculated for the chemical data, which is a measure of the strength of linear dependence between two variables. Statistical significance is given at either a 99% or 95% confidence level (CL). Q-mode factor analysis was used to identify common groups of elements referred to as factors. On the basis of XRD mineralogy and element correlations, each factor was assigned to represent a particular mineral or mineral group in the samples and elements in that factor are then associated with or contained within that mineral or group. This links the mineralogical environmental conditions and geochemical sources. Q-mode factor analysis was performed using Matlab script provided by Pisias et al. (2013). Each variable percentage was scaled to a percent of the maximum value before these values were row-normalized and cosine-theta coefficients calculated. Factors were derived from orthogonal rotations of principal component eigenvectors using the Varimax method (Klovan and Imbrie, 1971). All communalities, an index of the efficiency of a reduced set of factors to account for the original variance, are ≥ 0.90 .

The distribution of nodule abundance was determined using data collected by the Japan International Cooperation Agency and the Mining Agency of Japan from 1985 to 2000. Station numbers, latitude, longitude, water depth (m), and nodule abundance (kg/m^2) data from over 700 stations were compiled into a database and imported into ArcGIS 10.2 to create a distribution map using the Natural Neighbor method (Sibson, 1981). To quantify the Natural Neighbor distribution, a second interpolation transformed the map into a grid of cells, or pixels, each with a specific size ($x = y$) and an integer value for abundance. Since there are several stations where abundances are $< 1.0 \text{ kg}/\text{m}^2$, the values were converted to g/m^2 to ensure no lost data due to rounding. An associated attribute table containing abundance values and cell counts was generated and exported for calculations. All calculations were completed using the attribute table data and the cell size of the distribution map. The area encompassing a specific abundance belt (in km^2) was determined by multiplying the cell size by the cell count. A default cell size of 4327.18 m (18.7 km^2) for the abundance map was generated by the ArcGIS analysis. The resulting areas of each abundance value were summed to determine the total area (km^2) covered by the abundance distribution map within the EEZ; a total nodule tonnage was determined by multiplying those areas by their respective abundance value and summing. All calculations excluded the Manihiki plateau area due to a deficit of nodule abundance data for that region. Equations and explanation of the variables are in Supplementary Materials.

Concentrations of some elements in CIs nodules were compiled from Japanese analyses of nodules collected during their 1985–2000 cruises (JICA/MMAJ, 2001; Okamoto, 2003), as well as data from Usui and Mita (1994) and Landmesser et al. (1976), combined with the data presented here (Appendix 2) for archived nodules collected during several

cruises: C.I.G.M.F.V. RAVIKAI cruise of June 1976, MACHIAS cruise of November 1978, MACHIAS cruise of March 1980, and the MACHIAS cruise of April 1980. Along with the location and nodule abundance data, element contents for Co, Cu, Mn, Mo, Nb, Ni, Sc, Ti, V, W, Zr, and the \sum REY were compiled into individual databases to create distribution maps using ArcGIS. These maps were generated using the same methods as

the nodule abundance map. Maps were then compared and six $\sim 20,000 \text{ km}^2$ areas that show a variety of metal abundance combinations for different metals of economic interest were selected. That $\sim 20,000 \text{ km}^2$ area size was chosen because it is comparable to the size of the area that would currently be economically mineable within a contract license in the Clarion–Clipperton Zone (CCZ) nodule belt.

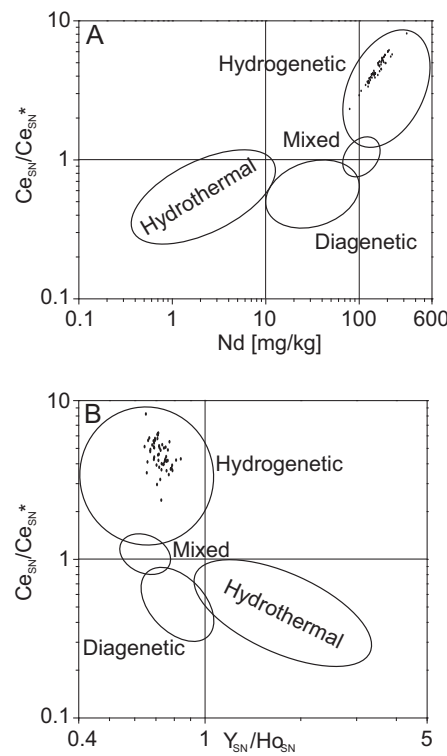


Fig. 2. Photographs of example Cook Islands Mn nodules used in this study. Pictured scale bars for A, B, C, D, F, J, K, and L are in cm, and the grid dimensions for E, G, H, and I are $5 \times 5 \text{ mm}$; (A) 12 ellipsoidal nodules with smooth surfaces from free-fall grab CK-76-1 STN-12 FFG-15; (B) 14 poly-nucleate nodules with smooth surfaces (CK-78-2 STN-08 FFG-16); (C) Four granular surface spheroidal nodules (CK-76-1 STN-11 FFG-14D); (D) Two flat nodules with granular surfaces (CK-78-2 STN-07 FFG-14A); (E) Six poly-nucleate nodules with a smooth-oxidized mm-thick surface layer missing in places on some samples (CK-78-2 STN-03 FFG-06); (F) Cross-section of a quarter of a nodule (CK-76-1 STN-07 FFG-10B) displaying interior structure and older Mn nodule fragment as a nucleus. (G) Interior of nodule U339 (20 mm) showing a relatively large, altered volcaniclastic rock nucleus; (H) Interior of nodule CK-76-1 STN-11 FFG-14D with moderate-sized mudstone nucleus; (I) Interior of sample CK-76-1 STN-11 FFG-14D with older Mn nodule fragment as the nucleus; (J) Interior of sample CK-76-1 STN-11 FFG-14A with small mudstone nucleus; (K) Interior of large ($\sim 80 \text{ mm}$) nodule (CK-78-2 STN-05 FFG-09A) with small mudstone nucleus; (L) Interior of sample G995 with mudstone nucleus and gray-brown mud that coats fracture or growth surfaces in some nodules.

Table 2

Statistics for chemical composition of Fe–Mn nodules, Cook Islands EEZ.

	Number	Mean	Median	St. dev ⁴	Min ⁴	Max ⁴
Fe wt.%	54	16.2	16.0	2.76	10.6	22.0
Mn	54	16.9	17.4	3.56	8.18	23.9
Fe/Mn	54	1.02	0.97	0.34	0.49	2.03
Si	54	8.03	7.12	2.43	5.50	16.8
Al	54	3.42	3.11	0.92	1.63	6.49
Mg	54	1.42	1.33	0.29	1.00	2.23
K	54	0.90	0.76	0.37	0.43	2.47
Ca	54	1.99	1.99	0.37	1.10	3.46
Na	54	1.76	1.79	0.24	1.14	2.37
P	54	0.34	0.34	0.06	0.18	0.53
Ti	54	1.28	1.23	0.34	0.77	2.11
LOI	54	27.7	28.0	3.15	20.1	33.4
H ₂ O [−]	54	12.7	12.0	4.46	6.60	21.0
H ₂ O ⁺	54	11.8	10.0	4.36	6.40	20.6
Ag ppm	49	0.23	0.21	0.11	0.05	0.46
As	54	150	148	29	84	247
Ba	54	1160	1201	210	638	1644
Be	54	3.9	4.0	0.77	2.3	5.6
Bi	54	11	12	3.2	5.1	18
Cd	54	4.7	4.2	1.9	1.6	11
Cl	54	4166	4836	3238	467	12,865
Co	54	3751	3933	945	1705	5408
Cr	54	59	21	125	1.1	644
Cs	54	<0.38	<0.34	<0.27	<0.10	1.6
Cu	54	2309	1877	1196	436	5625
Ga	54	<10	<9.8	<5.4	<0.10	24
Hf	49	13	13	2.8	8.0	21
In	54	0.78	0.82	0.25	0.33	1.3
Li	54	51	37	38	5.4	168
Mo	54	295	293	93	102	463
Nb	54	91	88	22	51	154
Ni	54	3767	3228	1814	1066	9257
Pb	54	976	918	292	442	1948
Rb	54	15	12	8.7	6.6	49
S	54	1829	1724	458	1003	2881
Sb	54	36	35	5.1	21	48
Sc	54	12	11	5.1	5.9	30
Se	54	<0.80	<0.76	<0.19	<0.20	1.22
Sn	54	7.8	6.8	4.3	3.0	28
Sr	54	935	973	156	466	1199
Ta	54	2.2	2.0	0.89	1.0	4.8
Te	54	24	25	8.9	8.6	41
Th	54	36	30	18	14	91
Tl	54	146	146	41	42	235
U	54	9.5	9.6	2.1	4.5	15
V	54	504	518	90	281	659
W	54	59	60	18	20	98
Zn	54	492	479	92	312	756
Zr	54	555	550	79	352	724
Hg ppb	28	<36	<22	<30	<5	117
Au	18	6	6	2	2	9
Ir	19	5	6	1	2	6
Os	11	2	2	1	1	3
Pd	19	7	6	3	2	11
Pt	19	232	224	59	141	328
Rh	19	17	17	4	8	27
Ru	19	18	19	2	12	23
La ppm	54	173	169	36.1	87.8	298
Ce	54	991	987	351	420	1993
Pr	54	40.9	39.7	9.17	20.9	74.7
Nd	54	160	160	38.1	79.3	323
Sm	54	34.7	34.2	7.50	17.5	63.9
Eu	54	8.53	8.48	1.91	4.06	16.5
Gd	54	36.1	36.3	7.37	18.0	65.4
Tb	54	6.09	6.11	1.39	2.90	11.4
Dy	54	34.9	34.9	7.00	17.4	62.4
Y	54	141	145	24.3	68.6	212
Ho	54	7.18	7.29	1.36	3.47	12.0
Er	54	19.1	19.4	3.43	9.27	29.8
Tm	54	3.02	3.08	0.58	1.39	4.68
Yb	54	19.8	20.3	3.86	8.86	32.5
Lu	54	2.98	3.10	0.56	1.42	4.46
ΣREY ¹	54	1678	1683	477.0	771.6	3205
%Heavy ²	54	17.2	16.2	3.02	13.1	24.7
Ce _{cn} ³	54	2.69	2.78	0.53	1.50	3.68
Ce _{sn} ³	54	2.65	2.73	0.52	1.47	3.64

**Fig. 3.** Data for Cook Islands nodules plot in the hydrogenic fields in discrimination graphs of (A) Ce_{Sn}/Ce_{Sn*} ratio vs Nd and (B) Ce_{Sn}/Ce_{Sn*} ratio vs Y_{Sn}/Ho_{Sn} ratios; discrimination plots from Bau et al. (2014).

Concentrations of the 11 metals and \sum REY and abundance data were extracted from each of the six areas using the “extract by mask” tool in ArcGIS. These data were used to calculate total dry tonnages of nodules, the number of possible 20-year mine sites in each area, and the total tonnage of each metal. The number of mine sites in each area is based on a production of 2.5 million dry metric tons of nodules per year, 50 million dry tons for 20 years; dry tons were converted from wet tons based on a mean of 27% moisture content ([JICA/MMAJ, 2001](#)). This choice of tonnage for a 20-year mine site falls within the high end of the range of other estimates used ([Yamazaki, 2008](#) and references therein). Total tons for the 11 metals and \sum REY within each area were calculated using attribute table data from the mine site abundance and element concentration maps. The default cell size for each element concentration map varies based on the ArcGIS’s Natural Neighbor analysis. Equations and the explanation of the variables are in Supplementary Materials.

3. Results

3.1. Sample description

The nodules analyzed range from 8 to 80 mm in diameter. Surfaces of the nodules range from black to dark-brown with granular to smooth textures. The nodules show two or three distinct concentric black layers

Notes to Table 2

¹ ΣREY = sum of rare earth elements plus yttrium.

² Percentage of the REY complement that are heavy REY (Eu through Lu).

³ Ce_{cn} is Ce anomaly normalized to chondrite values; Ce_{sn} is Ce anomaly normalized to PAAS values.

⁴ St. dev is standard deviation; Min is minimum; Max is maximum.

(Fig. 2). Most samples contain a thin laminated top layer, while others have an acicular top layer. The second layer can be acicular, mottled, or massive, and may contain a pale-brown mud patina. The third layer, if present, is acicular to porous, also with a pale-brown mud patina (Fig. 2). Nodules contain a nucleus of fish bone, shark's tooth, black dense older nodule fragment, gray, white, or pale-brown volcaniclastic/pyroclastic mudstone that is commonly zeolite rich, or altered basalt fragment; some mudstone nuclei can be large (Fig. 2). One group of nodules is polynucleate, while other groups are spherical to ellipsoidal (Fig. 2). Two pancake nodules, each with a large rock nucleus (encrusted volcaniclastic mudstone) are 31–54 mm thick. Both pancake

nodules (CK-76-1 STN-11 FFG-14C and CK-80-2 STN-17 WG-01B) have a botryoidal surface with a black granular micro-texture indicative of recent growth. Surface textures indicate that the pancake nodule CK-76-1 STN-11 FFG-14C was turned over at some point in its history. The pancake nodules have the same three layers as the other nodules.

3.2. Mineralogy

The manganese phase of all nodules analyzed is predominantly $\delta\text{-MnO}_2$, with lesser amounts of asbolane/buserite and birnessite. The $\delta\text{-MnO}_2$ has a high crystallinity and shows four X-ray reflections, rather

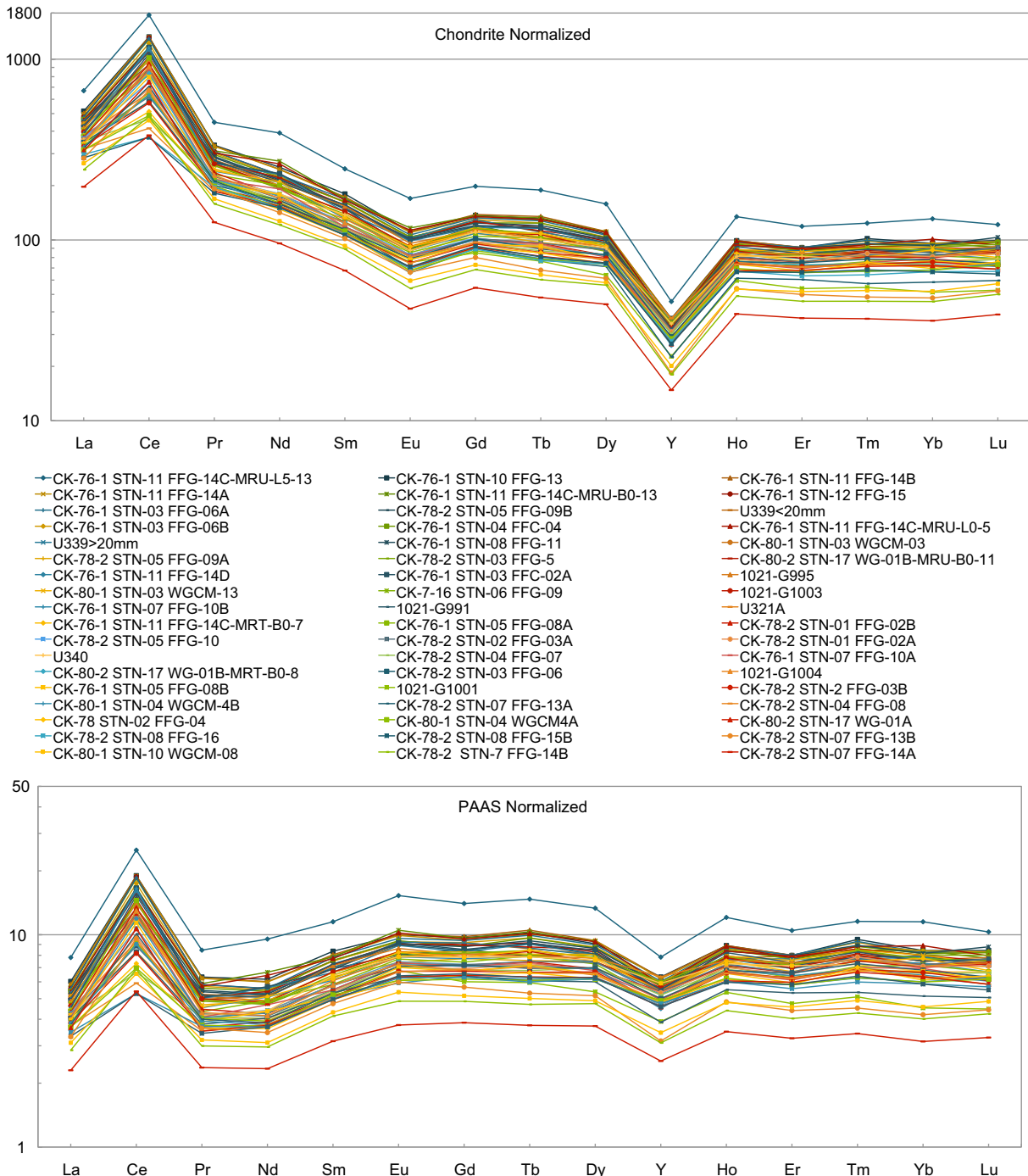


Fig. 4. Chondrite-normalized and PAAS-normalized rare earth element plots for bulk CI nodules showing large positive Ce anomalies and large negative Y anomalies, characteristic of hydrogenetic precipitation.

than the two reflections commonly found for most marine hydrogenetic manganese oxides. Asbolane and buserite cannot always be distinguished by XRD and where ambiguity exists, they are listed together in Supplementary Table S.1. The presence of 10 Å and 7 Å phyllo-manganates indicates that a small component of elements in the nodules was supplied from sediment pore fluids, but the dominant δ-MnO₂ in all samples indicates that the main source of metals was ambient seawater. The iron phase is X-ray amorphous for most samples, but minor goethite was detected in two samples (Supplementary Table S.1). Detrital quartz, plagioclase, and K-feldspar occur in most samples as well as authigenic phillipsite; clay minerals, especially nontronite, were detected in some samples, but it is likely that small amounts of smectite-group minerals occur in most samples, which with phillipsite are common alteration products of volcanic glass. The magnesium-rich clay mineral sepiolite found in many samples may also derive from alteration of volcanogenic material.

3.3. Chemical composition

Iron and Mn average 16.2% and 16.9% respectively for our dataset, and Fe/Mn ratios vary from 0.49 to 2.0 with an average of 1.0 (Table 2, Appendix 1), reflecting predominantly hydrogenetic precipitation. Hydrogenetic precipitation is verified by the Cls REY nodule data plotting in the hydrogenetic field on the discrimination diagrams of Bau et al. (2014); (Fig. 3). The aluminosilicate fraction (quartz, feldspars, phillipsite, clay minerals) varies by a factor of three, as represented by Si (5.50–16.8%); but the Si/Al ratio varies only from 1.8 to 3.4, indicating little change in the types of minerals and ratios of aluminosilicate minerals, only in the combined quantity of those minerals, which generally reflects the type and size of the nucleus.

The metals traditionally considered of greatest economic potential are Co, Ni, and Cu, which average in our dataset 0.38%, 0.38%, and

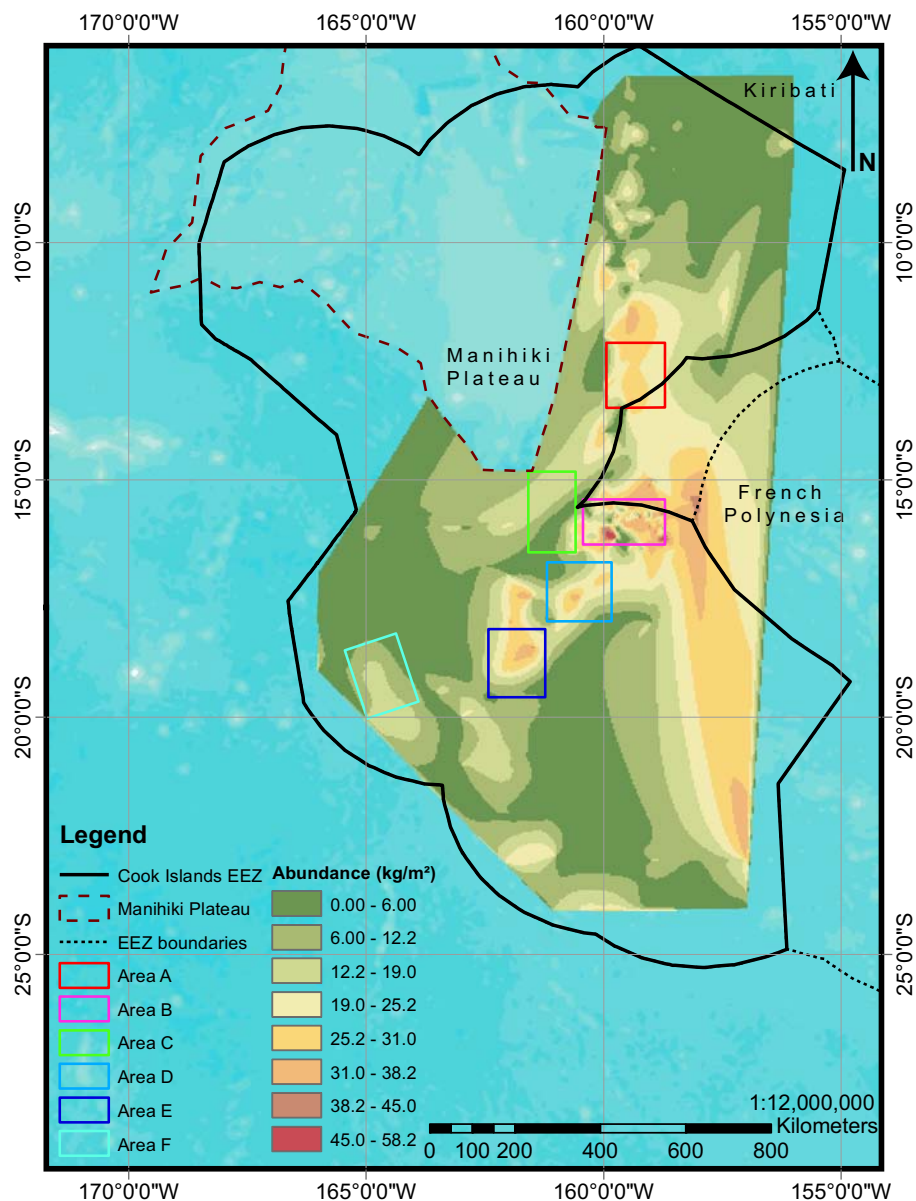


Fig. 5. Nodule abundance (kg/m^2) distribution map for Cook Islands based on data from Okamoto (2003) and JICA/MMAJ (2001); colored rectangles represent the locations of six areas that show a range of metal combinations of potential economic interest (see Figs. 6, 7, and supplementary Figs. S.1, S.2).

0.23% respectively. However, recent studies indicate that several other critical metals in Mn nodules and Fe–Mn crusts may be of economic interest, including Bi, Li, Mo, Nb, Te, Th, Tl, V, W, Zr, Pt, and the REY (Hein et al., 2013; Hein and Koschinsky, 2014). Of those critical metals, Bi, Li, and Th have concentrations too low in Cls nodules to be of economic

interest, but the other metals have been evaluated for economic potential (Tables 2, 3). In addition, Ti is higher in Cls nodules (average 1.28%) than in nodules found elsewhere (0.16%–0.42%; Hein et al., 2013; Hein and Koschinsky, 2014; see also Glasby et al., 1978) and Ti is also of economic interest. Finally, Sc, while occurring in the nodules only at the

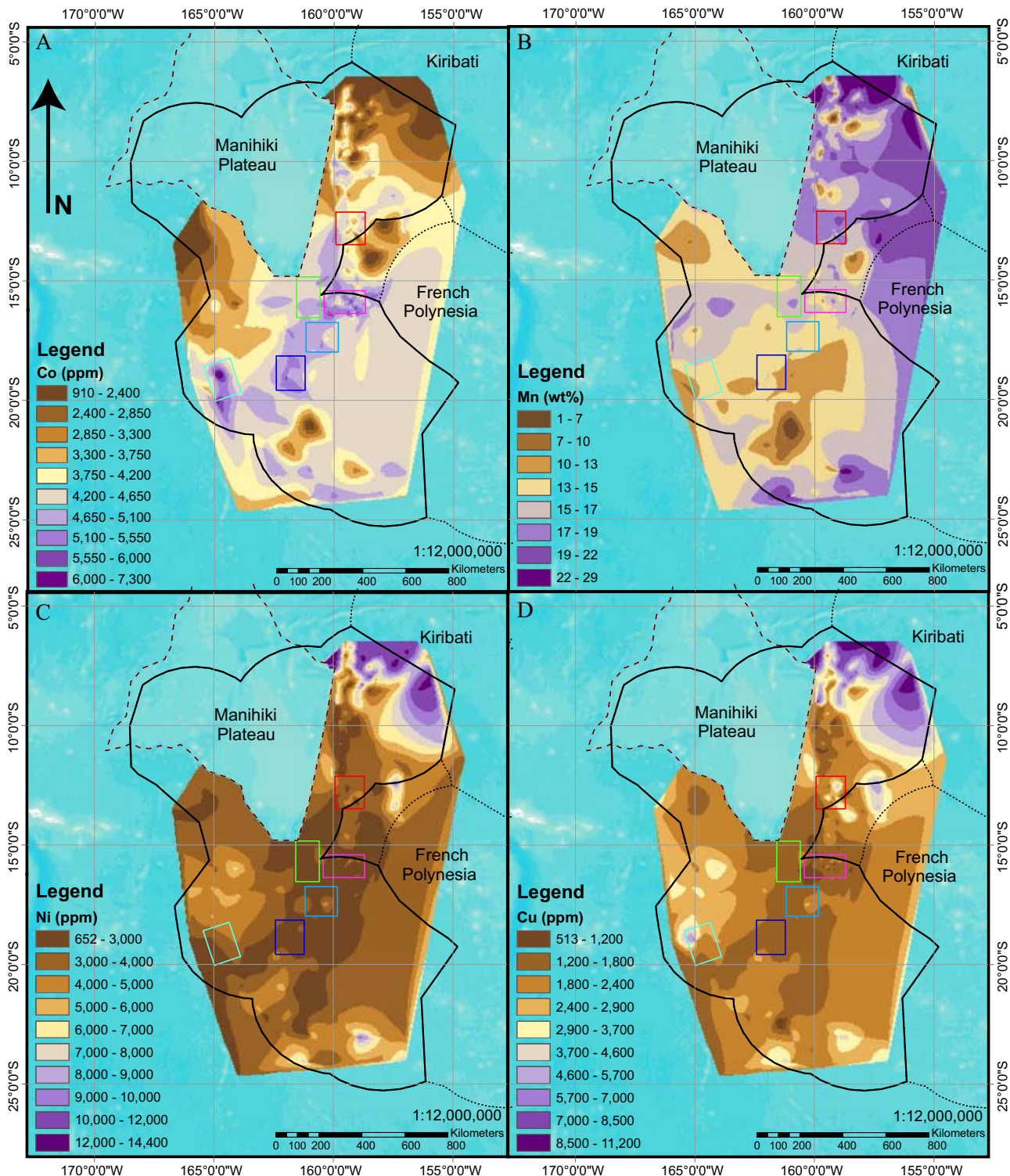


Fig. 6. Metal concentration distribution maps for (A) Co (ppm), (B) Mn (wt.%), (C) Ni (ppm), and (D) Cu (ppm) from Cook Islands nodules; colored rectangles are labeled in Fig. 5, and data within each rectangle are quantified in Table 3; concentration maps for Mo, W, Nb, Zr, V, and Sc are in supplementary Figs. S.1, S.2.

Earth's crustal average, may still be of economic interest because of its high global metal market price and the ease of extraction of metals from the ferromanganese (oxyhydr)oxide matrix (Hein et al., 2013). Like Ti, total REY contents (average 0.168%; maximum 0.321%) in Cls nodules are significantly higher than in nodules found elsewhere in the global ocean (0.040%–0.104%; Hein et al., 2013; Hein and Koschinsky, 2014; see also Glasby et al. (1978)). The Cls REY data plotted relative to chondrites (Anders and Grevesse, 1989) show light REY enrichments, positive Ce anomalies, and negative Eu and Y anomalies, and plotted relative to Post Archean Australian Shale (PAAS; McLennan, 1989) show the same Ce and Y anomalies and very small enrichments in middle and heavy REY (Fig. 4). The upper bounding sample (CK-76-1 STN-11 FFG-14C-MRU-L5-13) is the inner layer of a pancake nodule and has a relatively high Fe content and associated elements, including the highest As, Bi, Pb, and Th contents, whereas the lower bound sample (CK-78-2 STN-07 FFG-14A) has a high Fe/Mn ratio and the highest aluminosilicate component (Fig. 4).

3.4. Statistical analyses of chemical data

Manganese correlates at the 99% CL with Mo, W, Ti, Zn, Ni, Cu, Li and the five heaviest REEs (Ho–Lu) plus Y; whereas Fe at the same CL correlates with Th, Ti, Nb, all REY, Pb, Bi, Zr, Te, V, Co, and P. Elements also vary with both latitude and water depth, which are partially coupled because water depth increases to the north; some correlations common to both spatial parameters may have a causal relation with both latitude and water depth or with only one. Aluminum, Li, Cu, Rb, Ni, and Si have positive correlations with water depth and Ti, Ca, P, all REY, Co, Fe, Nb, Pb, Te, Th, and Zr have negative correlations with water depth. Lead and Zr also have positive correlations with latitude and therefore must relate to some process that varies with latitude and is not associated

with water depth. Latitude also has positive correlations with Th, Nb, Ti, Fe, Be, the light REEs, Ce anomaly (Ce^*), Bi, Co, and V and negative correlations with Na, Cu, Mo, S, K, Mn, Ni, and Tl.

Q-mode factor analysis identifies four factors that we interpret to represent the Fe, Mn, aluminosilicate, and biogenic (predominately phosphate) components, which account for 96% of the sample variance, 53%, 29%, 12%, and 2% respectively. The Fe phase shows the following associated elements listed by decreasing factor scores: Te, Co, Bi, V, Fe, Ce, U, Pb, Th, Zr, Nb, Lu, Tm, Ba, La, Yb, Er, Pr, Ho, Tb, Ti, Sm, Y, Sb, Gd, Eu, and Dy; the Mn phase shows: Cu, Mo, Mn, Ni, Zn, Li, Tl, W; the aluminosilicate minerals contain: Sc, Si, Al, Cr, K, Mg, Fe; and the biogenic, chiefly phosphate fish debris and shark's teeth, includes: Ti, Ca, P, Zr, Mg, Nb, Cl, Na. Although Mn shows positive correlations with the heavy REY, factor analyses places the REY only in the Fe factor.

3.5. Growth rates

Nodule growth rates were determined using the empirical equation of Manheim and Lane-Bostwick (1988): $GR = 0.68/(Co_n)^{1.67}$, where $Co_n = Co \cdot (50/Fe + Mn)$, with Co, Fe, and Mn in wt.%. The growth rate variability is small for the Cls nodules, 1.0–4.2 mm/Ma, mean 1.9 mm/Ma, which is in the same range as most hydrogenetic Fe–Mn crusts (Hein et al., 2000). The oxide portion on one pancake nodule was divided into two layers and the younger layer grew at a faster rate than the older layer, 1.95 mm/Ma compared to 1.4 mm/Ma. That change in growth rate would have occurred about 2.6 Ma ago, near the Pliocene–Pleistocene boundary. A nodule's radius divided by its growth rate produces ages for the initiation of the growth of large nodules of early to middle Miocene, about 18–14 Ma.

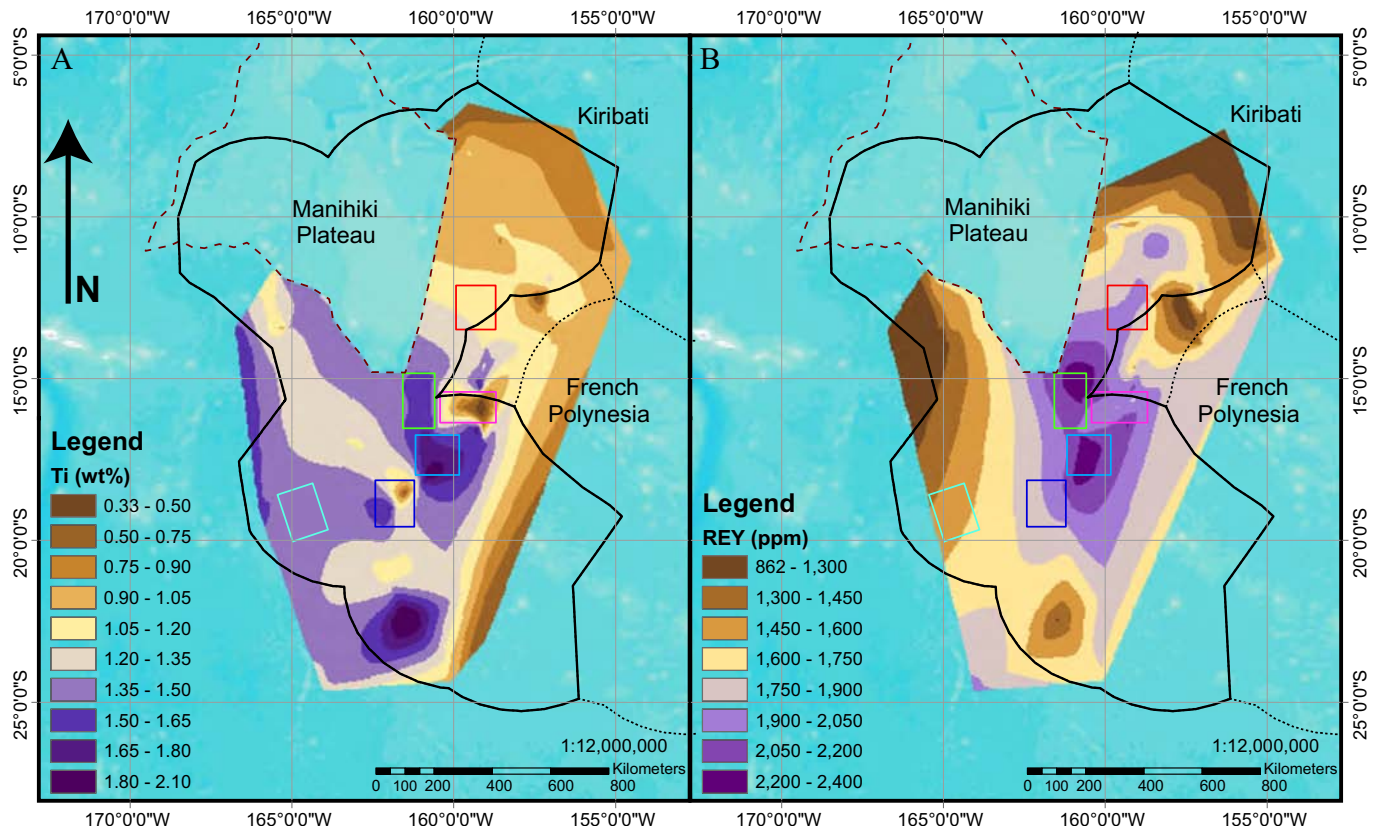


Fig. 7. Metal concentration distribution maps for (A) Ti (wt.%) and (B) \sum REY (ppm) from Cook Islands nodules; colored rectangles are labeled in Fig. 5, and data within each rectangle are quantified in Table 3.

3.6. Distribution of critical elements in the Cls EEZ

An abundance map in kg/m² of Mn nodules in the Cls EEZ shows a high abundance belt tending about N-S in the eastern part of the EEZ, which bifurcates, with a SW trending branch in the southern half of the EEZ (Fig. 5). Nodule abundance is very low through the NE sector of the EEZ. Very high nodule abundances of >25 kg/m² cover a huge area, about 123,844 km², which contains 3.61 billion wet tons of nodules. High Co contents in the nodules follow the SW branch and the northern part of the N-S main belt, with concentrations in places of over 0.7% Co (Fig. 6A). Manganese contents in the nodules are high in the NE sector where nodule abundances are low, and show only moderate concentrations in areas where nodules are high in Co (Fig. 6B). Nickel and Cu contents are also very high in the northern part of the NE

sector, up to 1.4% Ni and 1.1% Cu, where nodule abundances are low, and both are relatively low through the SW branch and the main belt of nodule abundance (Fig. 6C, D; see also Okamoto (2003)). Titanium and REY are high in nodules in the area of the intersection of the main belt and SW branch of nodule abundance and Ti is also high at the southern margin of the EEZ (Fig. 7A, B). Molybdenum and W have their highest contents in nodules located east of the Manihiki Plateau, whereas Nb and Zr have highest contents in the south-central EEZ. Vanadium has a poorly constrained, small high in the NE sector, and a moderate high at the intersection of the main belt and the SW branch of nodule abundance. Scandium shows two high areas, one adjacent to the SW flank of the Manihiki Plateau and the other at the SW margin of the EEZ. The western half of the EEZ shows average or higher Sc contents and the area east of the Manihiki Plateau shows below average

Table 3

Nodule and contained metal dry tons in six areas (Fig. 5) from the Cook Islands EEZ.

	Area A	Area B	Area C	Area D	Area E	Area F
Area (km ²)	20,316	19,324	20,541	20,372	20,466	20,297
Nodules (dry tons)	3.50×10^8	3.57×10^8	1.53×10^8	2.50×10^8	2.82×10^8	1.51×10^8
Number of 20 year mine sites ¹	7.0	7.1	3.1	5.0	5.6	3.0
Area of each 20 year mine site (km ²)	2902	2705	6706	4067	3626	6716
Area mined per year (km ²)	145	135	335	203	181	336
<i>Contained metal (dry tons)</i>						
Mn	61,002,292	56,029,138	23,635,308	34,824,492	37,984,935	20,992,979
Ti	4,144,400	3,584,071	2,350,609	4,173,565	3,614,946	1,951,593
Co	1,475,753	1,903,653	709,664	1,169,238	1,401,147	521,300
Ni	1,247,834	920,785	406,459	711,700	770,433	342,848
Cu	840,845	495,346	233,802	405,518	441,505	378,646
Σ REY	678,866	765,405	333,792	538,398	388,373	164,835
V	356,247	200,872	90,365	142,908	135,346	68,178
Zr	195,323	222,313	96,380	169,275	189,150	90,486
Mo	186,166	99,555	44,284	60,717	75,224	28,714
Nb	30,275	36,913	14,816	30,561	34,740	15,453
W	30,215	23,152	9943	15,700	16,074	5446
<i>Contained metal: dry tons per 20 year mine site¹</i>						
Mn	8,714,094	7,842,554	7,716,215	6,951,462	6,729,847	6,946,586
Ti	592,022	501,672	767,403	833,103	640,465	645,783
Co	210,809	266,460	231,684	233,396	248,243	172,499
Ni	178,251	128,885	132,697	142,065	136,499	113,449
Cu	120,114	69,335	76,329	80,947	78,222	125,294
Σ REY	96,975	107,136	108,973	107,472	68,809	54,544
V	50,889	28,117	29,501	28,527	23,979	22,560
Zr	27,902	31,118	31,465	33,790	33,512	29,942
Mo	26,594	13,935	14,457	12,120	13,328	9501
Nb	4325	5167	4837	6100	6155	5113
W	4316	3241	3246	3134	2848	1802
<i>Contained metal: dry tons in 1 year of production¹</i>						
Mn	435,705	392,128	385,811	347,573	336,492	347,329
Ti	29,601	25,084	38,370	41,655	32,023	32,289
Co	10,540	13,323	11,584	11,670	12,412	8625
Ni	8913	6444	6635	7103	6825	5672
Cu	6006	3467	3816	4047	3911	6265
Σ REY	4849	5357	5449	5374	3440	2727
V	2544	1406	1475	1426	1199	1128
Zr	1395	1556	1573	1689	1676	1497
Mo	1330	697	723	606	666	475
Nb	216	258	242	305	308	256
W	216	162	162	157	142	90
<i>Percentage produced in 1 year of 2013 global production</i>						
Mn	2.7%	2.5%	2.4%	2.2%	2.1%	2.2%
Ti	16%	13%	21%	22%	17%	17%
Co	9.6%	12%	11%	11%	11%	7.8%
Ni	0.42%	0.31%	0.32%	0.34%	0.32%	0.27%
Cu	0.04%	0.02%	0.02%	0.02%	0.02%	0.04%
Σ REY	5.1%	5.6%	5.7%	5.6%	3.6%	2.9%
V	4.0%	2.2%	2.3%	2.3%	1.9%	1.8%
Zr	0.10%	0.11%	0.11%	0.12%	0.12%	0.11%
Mo	0.53%	0.28%	0.29%	0.24%	0.27%	0.19%
Nb	0.31%	0.37%	0.35%	0.44%	0.45%	0.37%
W	0.30%	0.22%	0.22%	0.21%	0.20%	0.12%

¹ Based on 50×10^6 dry tons for a 20-year mine site, 2.5×10^6 dry tons per year.

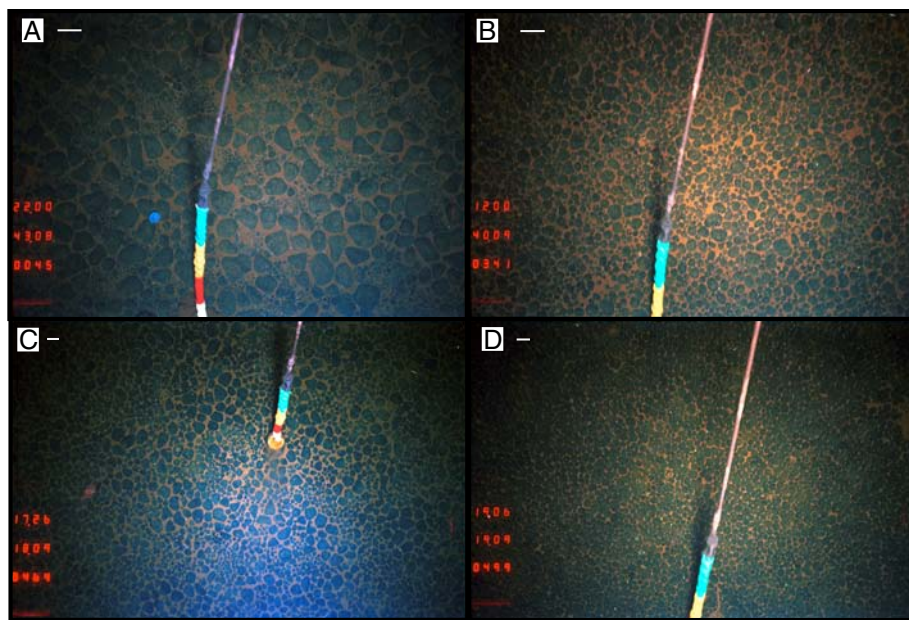


Fig. 8. Example seafloor images of Cook Islands nodule field taken on the 2000 Japanese Cruise (JIICA/MMA, 2001; Okamoto, 2003); (A) Photograph 0030, 4913 m; nodule area with 19 kg/m² and an average nodule size 5 cm; (B) Photograph 0325, 4946 m, with nodule abundance 20 kg/m² and average size of 5 cm; (C) Photograph 0447, 5009 m, with nodule abundance 25 kg/m² and average size of 4 cm; (D) Photograph 0482, 5009 m, with nodule abundance 30 kg/m² and average size of 4 cm; each bar scale represents 10 cm.

contents. Maps for Mo, W, Nb, Zr, V, and Sc are in the supplementary Figs. S.1, S.2.

3.7. Metal tonnages of selected areas of the Cls EEZ

The Cls EEZ contains about 12.1 billion wet tons of Mn nodules, excluding the Manihiki Plateau, which does not contain nodule abundances high enough to be of potential economic interest. Six areas (A–F) were chosen to represent a range of possible resource scenarios within the high nodule abundance zones of the Cls EEZ (Fig. 5). Each of those six areas is about 20,000 km² as described above and each would support 3–7 20-year mine sites. The area of each Cls 20-year mine site varies from 2705 to 6716 km², which translates into 135–336 km² mined per year (Table 3). The dry tonnage of contained metal mined per year varies from a high of 435,705 tons of Mn (Area A) to the lowest high of 216 tons for W (also Area A). Dry tonnage of contained \sum REY production per year would have a high for Area C, 5449 tons and nearly as high in Areas D and B, and a low for Area F, 2727 tons (Table 3).

Of the contained metals considered, Area A contains the highest dry tonnages of Mn, Ni, Cu, V, Mo, and W, Area B for Co, \sum REY, Zr, and Nb, and Area D for Ti (Table 3). This distribution changes somewhat when each area is divided into 20-year mine sites, in which case the highest Cu would be in a mine site in Area F, \sum REY in Areas C and B, and Zr and Nb in Areas D and E. Contained metals mined per year would be highest for Mn, Ni, Cu (and Area F), V, Mo, and W in Area A, Co in Area B, \sum REY is about the same in Areas B–D, Ti in Area D, and Zr and Nb in Areas D and E. These data show that through detailed exploration high-grade, high-tonnage productive mine sites for the metals of interest can be identified.

Projections of the percentage of annual global production of a metal produced from a Cls mine site is important to consider because a significant increase in supply will decrease the price in the global metal market. The percentage of the global production for the metals considered would be the highest for Ti, 13–22% and next for Co, 7.8–12%, and quite low for all the others (Table 3).

It should be emphasized that these calculations and evaluations are for contained dry metal, which will not be the same as the produced

metal. Ore tonnage will decrease, for example, during collection based on the efficiency of the mining equipment and grade will decrease depending on the efficiency of the extractive metallurgy. Other operations during the extraction, transport, and processing will decrease availability, grade, or tonnage. Considerations for biological reserve and refuge areas within the EEZ will also reduce the potentially minable area.

Table 4
Value (in USD) of contained metals in one dry ton of Cook Islands EEZ, nodules compared to CCZ nodules for select metals¹.

	Price of metal (\$/ton) ²	Mean content Cls nodules (g/ton)	Value in 1 ton Cls nodules (\$)	Value in 1 ton CCZ nodules (\$)
Manganese	2889	160,898	465	820
Σ REY ³	14,426,804	1665	263	176
Cobalt	29,604	4113	122	62
Titanium	8720	11,999	105	28
Nickel	17,140	3805	65	223
Scandium	5,000,000	12	61	53
Copper	7657	2262	17	82
Niobium	140,000	90	13	3
Platinum	54,294,362	0.21	11	7
Molybdenum	26,990	295	8	16
Vanadium ⁴	13,176	508	7	6
Tungsten	62,120	64	4	4
Tellurium	115,000	24	3	<1
Zirconium ⁴	3307	524	2	1
Total	–	–	1111	1447

¹ Italics, not included in the total, but may in the future be economic should global metal prices increase or efficacious metal extraction be developed, especially for Pt.

² 3-year average for Co, Cu, Mo, Mn, Ni, V, Pt, La, Ce, Pr, Nd, Sm, Eu, Tb, Dy, Y; 1.5-year average for W, Nb, and Te; 6 month average for Ti, Zr, Gd; Ti, Zr, Gd from metal-pages.com; Mo, Co, Ni, Cu from LME.com; Mn, Nb, Te, V, W, La, Ce, Pr, Nd, Sm, Eu, Tb, Dy, Y from asianmetal.com; Pt from platinum.matthey.com; spot quote for Ho, Er, Tm, Yb, Lu from stanfordmaterials.com; Sc quotes from \$3 to \$15 million found, arbitrarily chose \$5 million; price converted using exchange rate 1 rmb/kg to \$0.16/kg for Nb, Ti, W, and Zr; all >99% metal except for Mn (97.9%), Ti (99%), W (99.95%) metal.

³ Value for Σ REY based on sum of value for each individual rare earth to account for concentration variance and price differences.

⁴ Only oxide quotes found for V and Zr: V₂O₅ (98%), ZrO (98.5%).

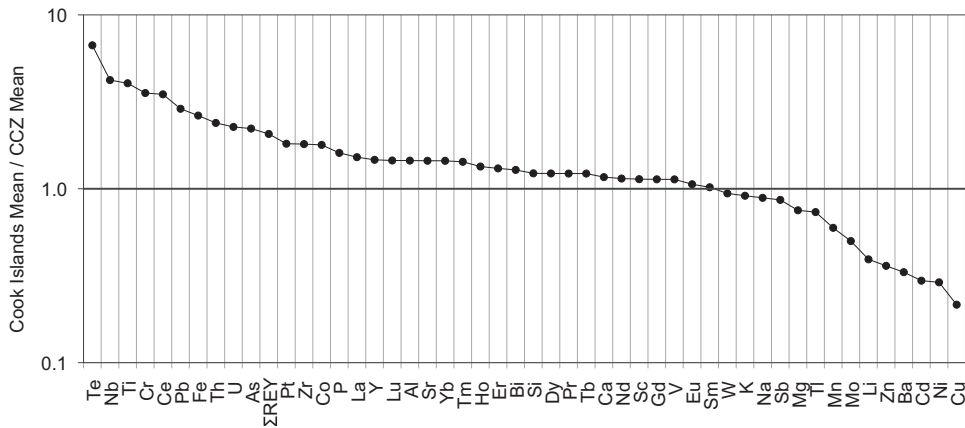


Fig. 9. Element enrichment diagram for mean composition of Cook Islands nodules relative to mean composition of Clarion–Clipperton Zone nodules from Hein et al. (2013); element ratios greater than 1 are enriched in the Cook Islands nodules and those below 1 are enriched in Clarion–Clipperton Zone nodules.

4. Discussion

4.1. Processes that control nodule and element abundances

The Cls EEZ has the highest concentration of nodules per square meter over the largest area in comparison to any other nodule field (Fig. 8A–D). Three things are generally required for the formation of Mn nodules, very slow rates of sedimentation, source of material to form a nucleus around which the oxide layers accrete, and a mechanism of turning the nodules so that they do not become buried. This latter criterion is important because even though the sedimentation rates are low, they are still 1000+ times faster than the growth rates of the nodules. Without turning, the nodules would eventually be buried, however, the Cls nodule field offers no conclusive evidence as to the mechanism for turning, as is also true for all other nodule fields. The interaction of biota with nodules (collisions) is the most often proposed mechanism for keeping nodules at the seafloor; Okamoto (2003) describes the benthic macrofauna and traces in the Cls nodule field.

Sediment in the Cls EEZ provides an abundant source of nuclei material shed from the Manihiki Plateau, small seamounts, and abundant shark's teeth and fish debris. Shark's teeth not only occur as nuclei, but are so abundant that they are also embedded in the oxide layers, and were found in nearly all the nodules analyzed here. This abundance of nucleus material combined with the slow sedimentation rates, subdued topography, and a branch of the Antarctic Bottom Water flowing through the Cls EEZ together support the growth of abundant nodules.

Cook Islands EEZ nodules form predominantly by hydrogenetic precipitation of Mn oxide and Fe oxyhydroxide from ambient bottom waters as indicated by their slow growth rates, chemical and mineralogical compositions, and by REY discrimination plots (Fig. 3). The chemical composition of the nodules varies throughout the Cls EEZ due to such factors as water depth, latitude, Fe/Mn ratios and resultant elements associated with each phase, and highly variable, and in places, very high contents of the aluminosilicate plus silica components. Water depth and latitude controls reflect changes in primary productivity, which within the Cls EEZ increases to the north toward the equatorial region. Higher primary productivity increases the depth of the calcite compensation depth (CCD), which significantly influences nodule composition (e.g. Cronan et al., 1991; Verlaan et al., 2004). The CCD is the depth at which the rate of supply and the rate of dissolution of biogenic calcite are equal and therefore no biogenic calcite accumulates on the seafloor. Above the CCD, biogenic calcite increases sedimentation rates and decreases the relative abundance of organic matter in the sediment. This affects the contents of the diagenetic associated metals in the nodules, which is a minor component in Cls nodules, except those forming in the far north of the EEZ. The highest-grade Cu–Ni–Mn nodules typically form near but generally below the CCD in

areas of high primary productivity (Cronan, 2006; Verlaan et al., 2004). The paucity of diagenetic input to the Cls nodules, which would otherwise promote high contents of Cu, Ni, and Mn, also controls the high Co and Fe contents in the Cls nodules. This is clearly seen in the high Fe/Mn ratios in Cls nodules (mean of 1) relative to diagenetic-component-rich CCZ nodules (mean of 0.2; Hein et al., 2013). So, even though most Cls nodules form near or below the CCD, surface-water primary productivity is low resulting in low organic matter content in the bottom sediments (Verlaan et al., 2004). Thus, the diagenetic reactions that are a rich source for Mn, Cu, and Ni are not occurring and therefore do not dilute the metals coming directly from seawater. Cobalt, Ti, and the other elements with seawater as their predominant source then become the dominant minor metals of economic interest. The combination of slow growth rates (mean 1.9 mm/10⁶ years) for the nodules and slow sedimentation rates (1–5 mm/10³ years; Verlaan et al., 2004) augment these processes that enrich the Cls nodules in Co, Ti, REY, and other hydrogenetic elements.

4.2. Comparison with CCZ nodule abundance and chemical composition

The CCZ is considered the area of greatest potential for the mining of Mn nodules, predominantly for Ni, Cu, and Mn. There are currently 15 exploration licenses with the International Seabed Authority in that area. Ore production of CCZ nodules and Cls EEZ nodules would provide

Table 5

Nodule abundance estimates (dry tons) and tonnages of contained metals, Cook Islands EEZ compared to CCZ nodules and global terrestrial reserves.

	All Cls nodules (1,133,075 km ²)	Cls nodules > 25 kg/m ² (123,844 km ²)	CCZ nodules ¹ (3,830,000 km ²)	Terrestrial reserves ²
Nodules (T)	8.86×10^9	2.63×10^9	21.1×10^9	–
Manganese ³	1.38×10^9	0.411×10^9	5.99×10^9	0.630×10^9
Titanium	108×10^6	32.0×10^6	67.0×10^6	420×10^6
Nickel	37.4×10^6	11.1×10^6	274×10^6	75.0×10^6
Cobalt	35.3×10^6	10.5×10^6	44.0×10^6	7.50×10^6
Copper	22.7×10^6	6.74×10^6	226×10^6	680×10^6
Σ REY	15.0×10^6	4.45×10^6	1.72×10^6	93.5×10^6
Zirconium	5.23×10^6	1.55×10^6	6.00×10^6	0.036×10^6
Vanadium	4.44×10^6	1.13×10^6	9.40×10^6	14.0×10^6
Molybdenum	2.34×10^6	0.694×10^6	12.0×10^6	11.0×10^6
Niobium	0.850×10^6	0.253×10^6	0.460×10^6	4.00×10^6
Tungsten	0.494×10^6	0.147×10^6	1.30×10^6	3.20×10^6
Tellurium	21.3×10^4	6.32×10^4	0.760×10^4	2.40×10^4

¹ From Hein et al. (2013).

² From U.S. Geological Survey (2013).

³ Dry metal tonnages calculated using element distribution maps (Figs. 5–7, SM), except tellurium which was determined using total nodule tonnage and average Te content in Table 4.

different commodities. CCZ nodules are a potential ore for Ni–Cu–Mn–Mo–(Co, Li), whereas the Cls potential ore would be Mn–REY–Co–Ti–(Ni, Sc) (Cronan, 2013; Hein and Petersen, 2013; Hein et al., 2013; Table 4). The elements of potential economic interest most enriched in Cls nodules relative to CCZ nodules are Te, Nb, Ti, Ce, \sum REY, Pt, Zr, and Co, whereas those most enriched in CCZ nodules are Cu, Ni, Li, Mo, and Mn (Fig. 9). Of the four metals with the largest global markets, Mn, Cu, Ni, and Ti, three are more enriched in the CCZ nodules, whereas most of the critical high-tech, green-tech, and energy application metals are more enriched in the Cls nodules, with the exception of Li.

Another significant difference is the vast area with high abundances ($>25 \text{ kg/m}^2$) of nodules in the Cls EEZ compared to the CCZ, which roughly averages about $5\text{--}6 \text{ kg/m}^2$ with an upper bound of 44 kg/m^2 (ISA, 2010), which compares to an average for the Cls EEZ of 14.4 kg/m^2 based on our Natural Neighbor ArcGIS analysis. This is an environmentally significant observation because a much smaller extraction area would be needed to supply the nodules for a 20-year mine site in the Cook Islands EEZ.

4.3. Resource and mining considerations

Cobalt and many of the other critical metals discussed here are currently produced as byproducts from the mining of land-based primary ores, such as from Cu, Fe, and Ni ores (Mudd et al., 2013). It is the demand for the focus metal that drives the production of the byproduct metal, which raises concerns about stable supplies for many byproduct metals. High-tech, green-tech, energy, and military applications have increased the demand for many of these byproduct metals and marine sources can augment the land-based supplies. Land-based supplies are not depleted and they will continue to supply the bulk of these resources for quite a long time, but advantages exist for deep-ocean mining that are driving this new industry forward to supplement the supply of byproduct metals from land-based production (Hein et al., 2013). For example, high grades, large tonnages, seabed exposures with little or no overburden to remove, moveable mining platforms so seabed infrastructure is minimal and can be relocated, no remote villages to move, no personnel at the mine site to be in danger; perhaps in addition, more easily processed ores for crusts and nodules and lower start-up costs, which taken together provide attractive incentives. Recent research in hydrometallurgy shows that selected metals or all metals in crusts and nodules can easily be put into solution and then selectively recovered (Pawel Plucinski, University of Bath, UK, oral presentation, Southampton, UK, February 2014). A pilot study to extract metals from marine ferromanganese oxides using hydrometallurgy was performed by Direct Nickel Ltd. (www.directnickel.com), which yielded recoveries for Ni, Co, Cu, Fe, and Mn of 98.9%, 92.2%, 99.6%, 90.8%, and 84.1% respectively (Malnic, 2008). Further breakthroughs in hydrometallurgy will be a key for the economic development of Mn nodules and crusts.

On the other hand, because deep-ocean mineral deposits have not yet been mined, the uncertainty of operations in a new environment is an important concern, and creates the perception of greater environmental issues than those associated with land-based mines. Transport to processing plants can also be long distance, 3200 km from the central Cls EEZ to New Zealand and 5700 km to Australia (Hein and Petersen, 2013). The same would apply to the CCZ nodules, in which case the distance from the central area of the CCZ to Baja California (Mexico) would be about 3000 km, and a processing plant would need to be built there. However, once loaded at the mine site in the Cls EEZ, the ore transport costs are not high on a per kilometer basis and if a processing plant were built in Mexico to process CCZ nodules, the 7000 km distance should not be prohibitive.

An additional advantage for the Cls EEZ specifically is that the seabed mud is stiffer and is not covered by a semi-liquid (soupy) seafloor layer, which is common in the CCZ and other nodule fields (Fig. 8A–D; see also

Okamoto (2003)). The predominantly red and brown clay of the Cls EEZ occurs throughout the high nodule abundance areas. Further, the red clays are indicative of oxic seafloor and sub-seafloor environments that, coupled with the low organic matter contents of the sediments, diminish redox reactions that can potentially release toxic elements and adsorb nutrients when the seabed is impacted during nodule extraction. These advantages, combined with the smaller areas that would need to be mined because of the high nodule abundances, may reduce the environmental impacts in the Cls EEZ compared to elsewhere.

4.4. Value of contained metals

The value of the contained metal in one ton of Cls EEZ nodules is about \$1111 USD (mean price over the last three years) based on Mn, \sum REY, Co, Ti, Ni, Sc, Cu, and Nb (Table 4). The results of such an estimate can vary significantly depending on the commodity priced. For example, much of the Mn on the market is sold as ferromanganese rather than Mn metal as priced in Table 4. We used metal prices for the chemical form that would most likely be extracted, although a favored extraction process has yet to be established. For the same contained metals, the value of one ton of CCZ nodules would be \$1447, although if Mo, which is more enriched in CCZ nodules, were switched for Nb, the value would be \$1460 USD. It is unlikely that one processor would extract all the metals listed, but down-stream processing could recover many of the important critical elements.

The Cls nodules have significantly more Mn, Co, Zr, and Te than the global terrestrial reserves (Table 5); this is true even if only the high tonnage belt ($>25 \text{ kg/m}^2$) is considered (Table 5). In addition, the Cls nodules contain about 50% of the terrestrial reserves of Ni, 32% of V, 26% of Ti, and 15–21% of REY, Mo, Nb, and W (Table 5). In addition, the complement of heavy REY of the total REY content averages 17% (maximum 24%; Table 2), which contrasts significantly with the <1% heavy REY in the large land-based carbonatite-hosted REY deposits (Hein et al., 2013)—it is the heavy REY that are most needed for high-tech applications. These large accumulations of metals in the Cls EEZ offer a secure supply of these critical commodities.

5. Summary

Cls Mn nodules form through hydrogenetic precipitation with little contribution from sediment pore waters (diagenetic contribution). The abyssal plain environment, along with water depth, latitude, primary productivity, sedimentation rates, abundance of nucleus material, and a mechanism for turning nodules are key to the unprecedented high nodule abundance and the unique suite of metals found in high concentration in these nodules. Although these nodules have relatively low contents of Ni (0.38%), Cu (0.23%), Li (0.005%), and Mn (16.9%) compared to the CCZ nodules, they possess high concentrations of other critical metals such as Co (0.38%), Ti (1.28%), and REY (0.168%). The Cls EEZ covers $1,977,000 \text{ km}^2$ and contains the highest concentration of nodules per square meter over the largest area of any nodule field in the global ocean, with $123,844 \text{ km}^2$ showing $>25 \text{ kg/m}^2$ nodule abundance yielding about 3.6 billion wet tons. This high nodule abundance is a great environmental advantage because smaller areas would be required to supply a potential 20-year mine site, resulting in lower environmental impact. The data presented here indicate that the Cls EEZ is potentially a world-class metal resource.

Supplementary data to this article can be found online at <http://dx.doi.org/10.1016/j.oregeorev.2014.12.011>.

Acknowledgments

We thank David Cronan, Imperial College London, Tracey Conrad, USGS, and an anonymous reviewer for their suggestions that improved this paper.

Appendix 1

Table A.1

Hygroscopic water-normalized (0% H₂O⁻) chemical composition of Cook Islands EEZ manganese nodules.

	CK-76-1 STN-03 FFC-02A	CK-76-1 STN-03 FFG-06A	CK-76-1 STN-03 FFG-06B	CK-76-1 STN-04 FFG-04	CK-76-1 STN-05 FFG-08A	CK-76-1 STN-06 FFG-08B	CK-76-1 STN-07 FFG-10A	CK-76-1 STN-07 FFG-10B	CK-76-1 STN-08 FFG-11	CK-76-1 STN-10 FFG-13	CK-76-1 STN-11 FFG-14A	CK-76-1 STN-11 FFG-14B	CK-76-1 STN-11 MRT-B0-7	CK-76-1 STN-11 MRU-B0-13	CK-76-1 STN-11 MRU-L0-5	CK-76-1 STN-11 MRU-L5-13	
Sample type	Nodule	Nodule	Nodule	Nodule	Nodule	Nodule	Nodule	Nodule	Nodule	Nodule	Nodule	Nodule	Nodule	PC Nod	PC Nod	PC Nod	
Description	B-1:29 ^a	B-1:35	B-3:22-25	B-1:27	B-1:40	B-2:16-23	B-4:22-28	B-2:24-29	B-0.13:43	B-1:47	B-1:35	B-1:30	B-1:25	B:0-7	B:0-13	L:0-5	L:5-13
Fe wt.%	19.6	19.7	20.4	19.4	17.0	16.6	17.4	16.9	16.3	17.4	19.4	21.1	20.6	17.4	20.2	22.0	19.1
Mn	15.6	17.9	16.8	17.7	17.8	17.4	17.9	18.2	18.4	20.4	17.9	16.8	16.3	14.3	15.1	14.5	15.3
Fe/Mn	1.26	1.10	1.21	1.10	0.96	0.95	0.97	0.93	0.88	0.85	1.08	1.26	1.27	1.22	1.33	1.52	1.25
Si	6.69	7.16	7.19	7.03	5.87	6.86	7.78	6.42	6.47	6.70	6.65	7.32	7.14	7.68	6.16	5.50	6.98
Al	2.79	3.09	3.13	3.11	2.49	3.01	3.50	2.93	2.57	2.81	2.84	2.98	2.83	3.14	2.20	1.63	2.60
Mg	1.16	1.26	1.33	1.31	1.15	1.27	1.38	1.29	1.18	1.22	1.25	1.27	1.24	1.09	1.09	1.00	1.02
K	0.60	0.71	0.68	0.64	0.59	0.63	0.81	0.64	0.72	0.70	0.72	0.70	0.69	0.79	0.55	0.43	0.74
Ca	1.93	2.11	2.04	2.03	1.91	2.16	2.09	1.90	1.98	2.20	2.02	2.13	2.06	2.11	1.94	1.84	1.90
Na	1.61	1.84	1.80	1.76	1.62	1.61	1.86	1.63	1.67	1.90	1.78	1.84	1.77	1.81	1.71	1.57	1.90
P	0.35	0.37	0.38	0.36	0.31	0.43	0.38	0.33	0.31	0.35	0.38	0.41	0.38	0.35	0.37	0.41	0.36
Ti	1.72	1.76	1.86	1.70	1.29	1.40	1.47	1.24	1.14	1.17	1.57	1.80	1.79	1.63	1.55	1.57	1.43
LOI	26.6	30.7	30.1	30.1	30.4	27.7	30.1	27.7	30.3	31.7	31.6	28.8	29.7	28.8	29.9	27.5	29.1
H ₂ O ⁻	9.90	20.3	19.4	18.2	10.8	10.1	17.7	10.5	11.8	19.7	19.2	18.2	18.1	10.5	11.9	7.40	12.2
H ₂ O ⁺	14.8	7.50	8.60	8.60	18.2	15.6	8.60	15.5	17.4	8.30	8.10	7.90	8.00	17.2	18.4	16.4	18.0
Ag ppm	0.18	0.30	0.33	0.33	0.13	0.18	0.30	0.18	0.15	0.29	0.33	0.32	0.38	0.12	0.17	0.13	0.21
As	180	161	165	164	163	147	145	172	178	171	172	172	177	145	209	185	247
Ba	1210	1368	1290	1357	1300	1224	1187	1080	1644	1357	1423	1296	1294	1263	1237	1231	1298
Be	4.2	3.6	3.7	4.2	4.3	4.0	3.4	3.6	4.8	4.0	4.3	4.3	4.3	4.6	4.4	4.3	4.6
Bi	14	14	15	13	13	12	11	13	15	14	14	15	15	11	16	15	18
Cd	3.5	3.3	3.5	3.9	3.8	5.0	4.3	4.6	4.1	3.8	3.7	3.3	3.5	2.9	2.8	2.5	2.5
Cl	710	7829	7630	7176	729	645	7108	715	760	7808	7079	8178	7387	849	953	918	945
Co	4473	4956	4529	4694	4608	3949	3827	4480	5408	4869	5173	4866	4835	3642	4813	3877	4442
Cr	18	29	26	23	4.5	20	23	6.7	11	17	20	32	35	28	20	14	17
Cs	0.22	0.38	0.37	0.37	0.22	0.22	0.36	0.22	0.23	0.37	0.37	0.49	0.37	0.22	0.23	0.22	0.23
Cu	1243	1443	1613	1834	1570	2214	2260	1888	1712	1818	1572	1333	1343	1486	1079	685	994
Ga	5.9	9.4	9.7	10	6.1	7.8	9.8	6.7	6.8	10	9.8	9.2	9.2	5.5	5.4	3.9	3.6
Hf	16	14	16	16	12	12	15	13	11	11	15	16	17	10	16	13	21
In	0.94	0.99	1.0	0.97	0.93	0.83	0.80	0.84	1.1	0.90	1.1	1.1	1.1	0.87	1.1	1.3	1.1
Li	22	21	26	32	25	40	41	34	28	22	26	20	18	13	10	5.4	8.0
Mo	238	300	251	293	277	255	286	292	359	390	323	249	249	230	272	281	245
Nb	112	110	124	119	90	90	101	95	93	83	114	125	127	69	115	91	129
Ni	2020	2723	2742	3227	2960	3526	3840	3229	3152	3362	3082	2482	2527	1877	1691	1695	1720
Pb	1354	1197	1278	1198	1188	1110	959	1229	1293	1161	1287	1345	1355	1094	1510	1339	1948
Rb	8.5	11	11	10	7.8	7.9	13	8.2	11	11	12	12	11	10	7.9	8.9	6.6
S	1554	2384	2233	2200	1570	1446	2187	1564	1927	2864	2351	2323	2198	1564	1589	1512	1595
Sb	39	35	37	36	36	35	32	37	40	33	38	42	43	31	47	38	48

Sc	9.1	12	12	12	8.0	8.2	12	7.9	9.4	12	13	14	14	9.6	9.2	8.1	7.9
Se	0.89	1.0	0.99	0.98	0.45	0.67	0.73	0.89	0.34	0.75	0.62	0.98	1.2	0.56	0.91	0.86	0.68
Sn	11	7.3	6.8	6.7	6.2	7.6	5.6	12	11	6.0	6.4	7.0	7.0	15	12	7.5	28
Sr	1000	1080	1066	1062	983	960	991	951	1179	1199	1105	1084	1089	943	1023	1078	1008
Ta	3.9	3.6	3.7	3.2	2.8	2.8	2.4	2.4	2.9	2.0	1.9	3.2	3.2	3.3	3.1	3.0	4.2
Te	35	36	31	32	37	29	25	30	41	33	34	33	32	27	36	31	32
Th	55	51	52	45	39	31	30	39	40	38	59	64	63	34	72	53	91
Tl	141	130	125	150	198	199	149	193	235	169	137	112	121	168	121	110	134
U	13	11	11	12	11	10	12	12	11	11	11	11	11	12	13	13	15
V	58	600	587	615	80	61	535	68	98	574	624	594	601	53	64	72	57
W	608	65	53	64	575	515	57	568	654	80	69	56	60	522	659	609	650
Zn	446	479	504	490	433	494	495	432	518	469	490	467	487	413	411	404	390
Zr	603	595	658	637	496	523	611	522	500	545	613	675	678	446	620	544	703
Hg ppb	117	–	–	–	47	47	–	49	85	–	–	–	–	57	58	94	18
Au	–	9	–	–	6	–	9	–	4	6	7	–	–	2	–	–	–
Ir	–	6	–	–	6	–	5	–	6	6	6	–	–	5	–	–	5
Os	–	3	–	–	–	–	2	–	–	1	2	–	–	–	–	–	–
Pd	–	10	–	–	5	–	11	–	5	7	11	–	–	5	–	–	2
Pt	–	211	–	–	242	–	196	–	327	214	205	–	–	146	–	–	148
Rh	–	16	–	–	21	–	15	–	27	17	17	–	–	14	–	–	16
Ru	–	23	–	–	20	–	17	–	18	20	20	–	–	18	–	–	16
La ppm	188	213	207	207	167	151	180	156	173	199	230	221	223	169	215	205	298
Ce	1321	1481	1390	1320	1155	907	984	989	1315	1245	1510	1504	1502	962	1464	1307	1993
Pr	44.6	51.4	50.5	49.5	38.3	34.3	43.7	36.1	40.0	48.3	55.8	55.0	55.3	40.3	52.0	50.5	74.7
Nd	193	189	186	183	166	148	160	159	172	178	209	203	204	173	226	218	323
Sm	38.2	43.4	41.7	42.1	32.4	28.1	35.8	30.5	33.9	40.2	46.4	44.1	44.7	34.4	43.6	42.9	63.9
Eu	9.89	10.4	10.0	10.1	8.30	7.58	8.82	7.98	8.49	9.78	10.8	10.7	10.8	8.94	11.3	11.0	16.5
Gd	39.7	43.8	42.8	41.1	34.6	31.3	38.2	33.0	35.9	41.0	45.2	43.9	45.7	36.5	44.8	44.5	65.4
Tb	7.06	7.69	7.48	7.47	6.15	5.57	6.52	5.73	6.11	7.25	7.90	7.78	8.13	6.55	7.99	7.84	11.4
Dy	39.5	41.9	40.9	40.6	34.1	30.6	36.6	31.7	34.9	40.3	42.5	43.9	44.0	36.3	43.5	43.4	62.4
Y	149	163	161	158	132	131	162	134	141	156	171	167	170	144	157	158	212
Ho	7.90	8.62	8.51	8.42	7.03	6.52	7.78	6.60	7.22	8.28	8.81	8.67	8.82	7.45	8.63	8.76	12.0
Er	20.4	22.8	22.5	21.9	17.8	16.9	20.4	17.4	18.8	22.7	22.8	22.7	22.8	19.1	21.9	22.1	29.8
Tm	3.17	3.76	3.60	3.57	2.87	2.74	3.41	2.84	3.04	3.61	3.85	3.73	3.58	3.04	3.43	3.56	4.68
Yb	22.4	23.3	23.7	23.0	20.3	19.0	21.7	19.6	20.7	23.0	23.8	23.0	23.2	21.8	23.7	25.1	32.5
Lu	3.11	3.61	3.60	3.57	2.89	2.67	3.27	2.69	2.89	3.80	3.65	3.57	3.63	2.94	3.35	3.44	4.46
ΣREY ¹	2086	2307	2199	2119	1825	1522	1712	1632	2014	2027	2391	2362	2370	1665	2326	2151	3205
%Heavy ²	14.5	14.3	14.7	15.0	14.6	16.7	18.0	16.0	13.8	15.6	14.2	14.2	14.4	17.2	14.0	15.2	14.1
Ce _{cn} ³	3.38	3.31	3.19	3.06	3.36	2.93	2.60	3.07	3.68	2.98	3.13	3.21	3.18	2.73	3.25	3.02	3.14
Ce _{sn} ³	3.33	3.26	3.13	3.01	3.33	2.91	2.56	3.04	3.64	2.93	3.07	3.14	3.12	2.69	3.20	2.96	3.08

¹ΣREY = sum of rare earth elements plus yttrium.²Percentage of the REY complement that are heavy REY (Eu through Lu + Y).³Ce_{cn} is Ce anomaly normalized to chondrite values; Ce_{sn} is Ce anomaly normalized to PAAS values.⁴B is bulk, L is layer; first number is number of nodules analyzed and the second and third numbers are maximum diameter of nodule or range of maximum diameter of nodules; Un is unknown because nodules were fragmented; PC Nod is pancake nodule; MRT is the most recent top and MRU is the most recent underside for pancake nodules

Table A.1 (continued)

	CK-76-1 STN-11 FFG-14D	CK-76-1 STN-12 FFG-15	CK-78-2 STN-01 FFG-02A	CK-78-2 STN-01 FFG-02B	CK-78-2 STN-02 FFG-03	CK-78-2 STN-2 FFG-03B	CK-78 STN-02 FFG-04	CK-78-2 STN-03 FFG-05	CK-78-2 STN-03 FFG-06	CK-78-2 STN-04 FFG-07	CK-78-2 STN-04 FFG-08	CK-78-2 STN-05 FFG-09A	CK-78-2 STN-05 FFG-09B	CK-78-2 STN-05 FFG-10	CK-78-2 STN-07 FFG-13A	CK-78-2 STN-07 FFG-13B	CK-78-2 STN-07 FFG-14A	CK-78-2 STN-7 FFG-14B	CK-78-2 STN-08 FFG-15B
Sample type	Nodule	Nodule	Nodules	Nodules	Nodules	Nodule	Nodule	Nodule	Nodule	Nodule	Nodule	Nodule	Nodule	Nodule	Nodule	Nodule	Nodule	Nodule	Nodule
Description	B-2:27-22	B-12:10-25	B-7:10-21	B-1/4:60	B-8:10-18	B-5:28-11	B-8:19-25	B ~ 6:Un	B-4:33-16	B-5:16-29	B-7:29-10	B-1:65	B-4:23-28	B ~ 4:Un	B-2:20-31	B-5:~18-20	B-2:18-33	B ~ 7:Un	B-11:20-13
Fe wt.%	19.8	20.4	14.7	15.2	14.0	13.6	12.9	16.1	13.9	12.0	11.3	16.2	16.8	15.1	16.7	17.9	13.4	14.8	14.7
Mn	15.6	16.1	21.1	19.6	22.3	19.8	23.9	20.9	19.4	23.3	23.2	19.9	17.5	14.8	11.1	8.83	8.30	10.1	12.6
Fe/Mn	1.28	1.27	0.70	0.78	0.63	0.69	0.54	0.77	0.71	0.51	0.49	0.81	0.96	1.02	1.51	2.03	1.62	1.46	1.16
Si	6.85	7.37	7.07	8.22	6.34	5.96	6.45	6.52	6.07	6.95	6.35	7.73	7.98	8.59	12.5	13.8	16.8	14.6	11.6
Al	2.79	3.09	3.49	3.30	3.30	2.97	3.45	3.08	3.09	3.58	3.44	2.99	3.44	3.71	4.93	5.27	6.49	5.95	5.10
Mg	1.20	1.45	1.57	1.31	1.80	1.60	2.07	1.44	1.59	2.03	2.11	1.33	1.41	1.29	1.59	1.62	1.63	1.73	1.49
K	0.67	0.70	0.76	0.91	0.73	0.63	0.74	0.73	0.69	0.97	0.84	0.86	1.03	1.03	1.71	1.28	2.47	1.54	1.35
Ca	1.96	1.92	2.18	2.17	2.24	1.97	2.12	2.20	2.16	2.12	2.19	2.12	2.21	1.89	1.28	1.12	1.10	1.24	2.03
Na	1.70	1.74	1.88	2.01	1.80	1.64	1.83	1.82	1.66	2.05	1.81	1.93	1.83	1.62	1.54	1.52	1.48	1.55	2.06
P	0.37	0.36	0.35	0.33	0.39	0.32	0.32	0.38	0.44	0.34	0.39	0.33	0.50	0.33	0.27	0.25	0.18	0.23	0.32
Ti	1.69	1.95	1.14	1.05	1.07	1.01	0.98	1.18	1.05	0.84	0.81	1.13	1.33	1.22	1.35	1.33	0.86	1.02	1.64
LOI	27.6	28.6	28.7	30.9	26.7	27.9	27.8	31.1	26.8	28.0	23.5	32.1	27.4	26.1	22.0	21.9	20.5	23.2	20.1
H ₂ O ⁻	11.9	17.5	16.7	18.7	13.7	6.60	15.9	19.0	6.80	15.2	7.20	20.8	15.1	6.90	11.0	11.4	12.0	13.4	7.90
H ₂ O ⁺	16.3	8.50	8.60	7.70	8.80	15.3	8.30	7.20	14.8	7.90	11.0	7.10	7.70	15.0	7.50	7.00	6.40	7.20	9.90
Ag ppm	0.16	0.36	0.26	0.26	0.25	0.16	0.19	0.36	0.10	0.21	0.10	0.28	0.45	0.08	0.46	0.44	0.26	0.31	0.12
As	176	170	131	134	131	133	118	154	124	131	119	163	160	146	131	130	84	103	109
Ba	1192	1321	1297	1378	1251	1124	1272	1370	1031	1215	1131	1465	1284	1059	828	756	638	702	777
Be	4.2	4.1	3.4	3.9	3.0	3.4	2.6	4.4	3.2	2.8	2.6	4.9	4.2	3.7	3.3	3.4	2.3	2.7	3.3
Bi	15	15	11	13	9.9	8.9	8.2	12	8.9	8.1	6.7	14	11	9.6	7.5	7.4	5.1	6.1	5.7
Cd	3.4	3.7	6.2	4.2	7.1	6.9	8.6	5.4	6.7	11	10	4.4	4.7	3.9	3.7	2.7	2.8	3.4	5.2
Cl	783	7467	6867	8155	6014	621	5826	6963	655	6533	560	7816	6396	623	5011	4628	3761	4342	467
Co	4449	4824	3806	4034	3407	3597	2794	4111	3369	2583	2909	4141	3922	3824	2742	2393	1705	2079	1933
Cr	23	32	19	17	19	36	21	21	14	20	14	16	33	52	342	426	644	498	52
Cs	0.34	0.48	0.36	0.37	0.35	0.21	0.36	<0.1	0.21	0.12	0.22	0.25	0.24	0.32	0.79	1.13	1.59	1.27	0.43
Cu	1317	1867	3445	2571	4137	3458	5113	3086	3208	5625	5593	2146	2497	1944	1663	1298	1580	1744	2465
Ga	5.8	10	12	10	13	9.2	15	12	8.3	21	14	15	12	7.2	12	12	12	8.9	
Hf	17	18	12	11	12	13	9.5	12	14	9.4	9.7	11	16	15	15	15	8.0	9.2	15
In	1.1	1.1	0.67	0.98	0.54	0.49	0.48	0.77	0.55	0.42	0.33	1.0	0.84	0.72	0.63	0.56	0.43	0.47	0.40
Li	19	36	80	33	107	90	134	51	77	136	150	29	44	37	58	52	76	73	88
Mo	241	239	373	370	417	391	449	374	355	436	463	408	329	298	146	103	116	133	132
Nb	119	154	84	84	83	76	73	89	83	60	58	90	120	97	92	89	51	60	88
Ni	2406	3188	5654	4071	6941	4593	8537	5173	4324	9257	7231	4331	4594	2793	2899	1986	2466	2806	2693
Pb	1396	1358	866	847	899	806	751	856	770	712	724	848	931	905	742	743	442	562	592

Rb	9.1	13	11	14	11	8.5	11	12	8.6	15	11	14	18	14	32	39	49	41	20
S	1476	2061	2881	2460	2317	1713	2259	2469	1609	2123	1616	2399	2120	1504	1461	1242	1136	1270	1086
Sb	44	45	36	36	35	35	36	37	35	39	34	41	42	36	33	32	21	26	32
Sc	9.2	14	11	12	10	6.7	9.0	11	6.5	9.8	5.9	14	13	9.9	22	28	30	27	11
Se	0.91	0.73	0.48	<0.2	0.70	0.86	0.71	0.99	0.86	1.1	0.86	0.76	0.94	0.86	1.0	0.68	0.68	0.58	0.76
Sn	7.4	13	4.6	5.5	5.7	7.5	4.6	21	3.0	10	5.1	7.3	6.9	4.5	5.2	5.9	3.0	3.7	16
Sr	1019	1017	1023	1005	970	905	898	1062	817	975	883	1141	934	859	681	633	466	567	708
Ta	3.3	3.8	1.7	1.8	1.4	1.5	1.3	1.9	1.3	1.2	1.0	2.0	2.0	1.8	2.0	2.1	1.1	1.4	2.4
Te	34	30	21	34	17	17	14	24	19	10	11	38	21	22	15	14	11	13	10
Th	60	69	19	21	19	18	15	24	18	15	14	24	34	32	44	48	20	27	22
Tl	143	106	166	173	181	173	184	184	182	210	223	167	140	135	75	55	63	73	98
U	12	10	9.5	8.6	9.5	9.6	8.4	10	9.5	8.0	8.8	9.2	9.5	9.2	6.7	6.3	4.5	5.8	7.7
V	56	608	490	520	492	77	473	538	60	479	71	566	581	53	425	391	281	323	24
W	583	53	72	76	76	439	80	70	425	71	419	78	60	444	28	20	20	24	358
Zn	455	509	711	481	637	551	721	567	520	756	730	481	498	406	447	432	380	433	423
Zr	614	724	561	528	561	496	510	612	515	476	430	577	700	539	578	565	352	433	516
Hg ppb	50	-	-	-	-	19	-	-	15	-	46	-	-	29	-	-	-	-	64
Au	-	7	-	6	5	-	5	-	-	-	-	6	7	2	-	-	-	-	-
Ir	-	6	-	5	6	-	6	-	-	-	-	4	6	5	-	-	-	-	-
Os	-	2	-	1	1	-	2	-	-	-	-	3	2	-	-	-	-	-	-
Pd	-	6	-	7	6	-	6	-	-	-	-	6	6	4	-	-	-	-	-
Pt	-	232	-	284	307	-	328	-	-	-	-	303	272	214	-	-	-	-	-
Rh	-	17	-	17	21	-	24	-	-	-	-	16	18	16	-	-	-	-	-
Ru	-	19	-	20	19	-	19	-	-	-	-	18	20	16	-	-	-	-	-
La ppm	190	213	160	165	161	147	140	194	155	157	142	196	210	163	144	126	87.8	109	127
Ce	1283	1491	778	1065	703	651	583	930	661	528	471	1152	1059	853	803	764	431	547	420
Pr	44.3	51.4	36.3	39.4	37.4	32.4	32.2	43.0	33.5	36.2	31.1	43.6	47.6	36.6	35.3	32.1	20.9	26.4	30.3
Nd	191	189	136	144	140	132	122	159	137	137	128	162	176	149	130	117	79.3	100	125
Sm	36.9	41.9	29.9	32.3	30.6	28.4	27.5	34.7	29.3	30.4	27.9	35.2	38.4	32.0	29.6	26.3	17.5	23.0	27.5
Eu	9.61	10.1	7.64	7.58	7.91	7.27	6.59	8.57	7.67	7.64	7.22	7.98	8.69	8.06	6.82	6.46	4.06	5.25	6.92
Gd	38.7	41.7	32.2	33.5	33.6	31.4	30.1	39.3	33.6	31.8	32.0	36.0	39.7	33.8	29.8	26.4	18.0	22.6	30.5
Tb	6.99	7.09	5.65	5.78	5.79	5.15	5.12	6.21	5.38	5.25	5.10	5.85	6.12	5.56	4.70	4.11	2.90	3.64	4.86
Dy	37.7	38.8	32.2	32.3	34.6	31.3	29.0	37.7	32.7	32.8	30.8	35.0	38.2	32.4	28.1	24.2	17.4	22.2	29.3
Y	149	145	144	145	146	127	130	157	135	140	129	150	160	125	104	85.3	68.6	83.6	124
Ho	7.60	7.55	6.94	7.07	7.16	6.53	6.11	7.77	6.73	6.82	6.52	7.35	7.62	6.64	5.46	4.79	3.47	4.35	5.92
Er	19.8	20.5	18.6	18.9	19.0	17.9	16.6	20.9	18.8	18.2	17.8	19.8	20.5	17.6	15.2	12.5	9.27	11.5	16.6
Tm	3.11	3.30	3.18	3.05	3.17	2.78	2.84	3.48	2.96	2.83	2.77	3.09	3.13	2.78	2.17	1.83	1.39	1.73	2.58
Yb	22.1	21.2	20.0	19.8	20.3	18.7	17.2	22.6	19.2	18.5	18.0	20.2	20.5	17.7	14.5	11.9	8.86	11.3	16.5
Lu	3.11	3.30	3.09	3.15	3.34	2.63	2.77	3.47	2.74	2.87	2.53	3.07	3.20	2.53	2.19	1.92	1.42	1.84	2.38
ΣREY^1	2041	2286	1413	1722	1354	1241	1151	1667	1281	1156	1052	1876	1838	1486	1356	1246	772	974	969
%Heavy ²	14.6	13.1	19.4	16.0	20.8	20.2	21.4	18.4	20.7	23.1	23.9	15.4	16.7	16.9	15.7	14.4	17.5	17.2	24.7
Ce _{cn} ³	3.27	3.34	2.38	3.10	2.12	2.19	2.02	2.37	2.13	1.64	1.64	2.90	2.47	2.56	2.65	2.83	2.35	2.39	1.59
Ce _{sn} ³	3.23	3.28	2.36	3.05	2.09	2.18	2.00	2.35	2.12	1.62	1.63	2.88	2.45	2.54	2.60	2.77	2.32	2.35	1.56

Table A.1 (continued)

	CK-78-2 STN-08 FFG-16	CK-80-1 STN-03 WGCM-03	CK-80-1 STN-03 WGCM-13	CK-80-1 STN-04 WGCM-04A	CK-80-1 STN-04 WGCM-04B	CK-80-1 STN-10 WGCM-08	CK-80-2 STN-17 WG-01A	CK-80-2 STN-17 WG-01B-MRT-B0-8	CK-80-2 STN-17 WG-01B-MRU-B0-11	1021-G991	1021-G995	1021-G1001	1021-G1003	1021-G1004	U321A	U339 < 20 mm	U339 > 20 mm	U340
Sample type	Nodule	Nodule	Nodule	Nodule	Nodule	Nodule	Nodule	PC Nod	PC Nod	Nodule	Nodule	Nodule	Nodule	Nodule	Nodule	Nodule	Nodule	Nodule
Description	B-14:10-20	B-2:-28-30	B ~ 3:-33-15	B-5:12-23	B ~ 9:-8-20	B-1:48	B-2:32-~ 20	B:8	B:11	B-1:28	B-1:31	B-1:42	B-1:32	B-1:38	B-1:30	B-4:15-19	B-1:30	B-1:37
Fe wt.%	14.1	17.0	15.8	11.4	12.7	10.6	13.8	14.3	16.2	19.0	16.3	16.3	15.2	13.7	13.1	17.4	16.5	13.6
Mn	13.7	19.9	18.7	21.7	19.2	16.2	17.7	17.4	18.8	13.8	14.7	8.18	15.5	18.7	16.3	17.0	15.7	14.5
Fe/Mn	1.03	0.85	0.85	0.52	0.66	0.65	0.78	0.82	0.86	1.38	1.11	1.99	0.98	0.73	0.80	1.02	1.05	0.94
Si	11.2	7.10	6.77	7.89	9.68	12.9	7.71	7.39	7.58	7.45	6.36	11.27	6.86	6.17	8.77	7.01	6.96	11.34
Al	5.07	3.06	2.94	4.20	4.24	4.74	3.67	2.95	2.94	3.57	2.92	3.62	3.21	3.10	3.88	2.65	2.48	4.53
Mg	1.57	1.24	1.22	2.09	1.73	1.85	1.36	1.14	1.22	1.21	1.25	2.23	1.29	1.43	1.45	1.35	1.18	1.35
K	1.28	0.83	0.80	1.18	1.26	1.73	0.84	0.77	0.85	0.73	0.62	0.97	0.66	0.59	1.18	0.80	0.92	1.73
Ca	2.46	2.74	1.86	1.71	1.73	1.45	1.87	1.96	1.96	1.52	1.80	3.46	1.72	1.94	1.90	2.64	2.04	2.01
Na	2.06	1.92	1.79	2.12	2.13	2.37	1.79	1.80	1.91	1.24	1.14	1.51	1.21	1.27	1.95	1.79	1.77	2.29
P	0.47	0.33	0.30	0.29	0.29	0.21	0.28	0.28	0.31	0.34	0.34	0.32	0.32	0.31	0.35	0.53	0.37	0.39
Ti	1.52	1.05	0.99	0.77	0.81	0.82	0.94	0.91	0.95	1.32	1.28	2.11	1.10	1.00	0.90	1.44	1.37	1.04
LOI	23.7	33.0	26.4	28.3	29.2	25.1	26.9	29.2	24.5	27.5	31.4	23.0	33.4	30.5	26.4	25.2	29.9	23.1
H ₂ O ⁻	11.8	21.0	8.20	15.9	17.9	13.9	7.80	7.60	8.70	10.3	8.90	7.50	10.0	9.90	8.30	8.60	8.70	9.70
H ₂ O ⁺	7.9	7.40	13.7	7.90	7.00	7.10	15.3	17.3	12.2	16.3	20.6	12.5	19.9	17.6	13.7	12.3	17.5	10.1
Ag ppm	0.37	0.38	0.09	0.23	0.21	0.21	0.09	0.12	0.05	—	—	—	—	—	0.16	0.20	0.18	0.17
As	111	166	155	124	133	101	126	134	153	191	178	126	173	166	128	146	150	125
Ba	925	1380	1176	1189	1158	947	1011	1169	1391	971	1008	701	996	1110	1073	1225	1117	947
Be	3.2	4.9	4.2	2.9	3.5	2.8	3.9	4.7	4.9	5.6	5.4	3.2	5.0	5.0	3.6	4.3	4.3	3.2
Bi	6.3	13	13	8.0	9.6	6.8	11	10	13	13	14	7.1	12	12	7.8	11	10	6.9
Cd	6.2	4.4	4.6	9.7	6.8	6.8	5.7	4.1	3.4	4.8	4.4	1.6	5.1	6.7	5.2	3.6	2.9	4.3
Cl	4660	7772	730	7004	7296	6039	662	736	811	5753	5280	12865	5822	5727	687	842	734	642
Co	1871	3962	3943	2699	2801	2056	3623	3766	4009	3489	4391	3395	4533	4528	2694	4267	4140	2326
Cr	71	11	1.1	14	19	29	5.4	8.7	19	17	24	144	16	13	24	60	37	28
Cs	0.34	<0.1	0.22	0.24	0.37	0.46	0.22	0.32	0.33	0.56	0.66	0.54	0.56	0.44	0.22	0.33	0.33	0.33
Cu	3345	2506	2342	5482	3666	4065	2527	2078	1774	1672	1570	436	1778	2220	2683	1849	1588	2237
Ga	13	11	3.9	20	18	21	5.5	5.1	3.8	19	18	17	20	24	5.9	<0.1	0.11	5.3
Hf	11	13	15	9.5	9.7	9.3	12	11	13	—	—	—	—	—	9.8	14	12	10
In	0.45	0.95	0.84	0.45	0.57	0.48	0.74	0.75	1.10	1.1	0.92	0.39	0.84	0.78	0.56	0.75	0.71	0.45
Li	103	32	35	168	91	85	57	32	27	51	37	16	51	78	68	22	13	50
Mo	137	385	414	422	395	308	330	356	398	213	239	102	277	340	322	232	256	268
Nb	79	87	87	65	69	56	74	63	82	108	120	108	107	82	71	85	74	76
Ni	3776	3962	3214	8609	6577	6725	3449	2749	2705	2832	3282	1066	4078	4795	4329	3304	2694	3488
Pb	586	999	1046	684	716	515	893	882	1023	992	1041	638	949	968	735	897	826	703
Rb	26	14	12	19	21	29	13	11	12	13	12	17	13	10	18	12	14	26

	1701	2532	1852	1902	1949	1510	1735	1840	2191	1003	1207	1405	1222	1221	1636	2079	1972	1550
Sb	33	38	35	39	38	31	34	29	31	34	35	27	36	34	30	34	34	29
Sc	14	12	8.2	11	13	16	7.6	6.9	7.7	16	15	19	16	13	11	11	10	11
Se	0.68	0.89	0.87	0.83	0.97	0.70	0.76	0.65	0.55	0.78	0.77	0.65	0.67	0.44	0.76	0.66	0.99	0.89
Sn	6.6	6.7	9.4	4.3	5.4	6.9	5.9	5.5	7.4	7.1	6.9	8.0	6.2	6.1	5.6	9.1	7.6	5.3
Sr	823	1081	991	818	865	708	854	1005	1117	769	804	836	774	860	833	1073	1084	803
Ta	2.1	1.7	1.7	1.1	1.4	1.3	1.5	1.8	1.6	2.0	2.4	4.8	1.9	1.3	1.5	1.9	2.3	1.7
Te	8.6	27	25	12	17	10	22	27	31	15	23	16	27	24	17	29	27	16
Th	22	29	29	16	18	17	26	27	29	70	43	39	45	39	21	24	24	25
Tl	113	165	178	164	141	142	180	162	172	97	137	42	133	189	158	154	133	122
U	7.0	9.9	11	6.9	6.7	5.5	9.3	9.7	11	8.5	8.7	6.2	8.1	7.8	8.2	10	11	8.1
V	385	558	73	460	459	367	55	60	83	531	523	390	520	493	56	50	49	44
W	26	71	526	76	68	48	407	442	515	40	48	21	54	67	414	457	447	405
Zn	552	486	420	698	566	515	479	437	440	650	625	546	604	484	484	473	433	416
Zr	524	624	578	490	505	423	482	403	558	–	–	–	–	–	531	616	553	540
Hg ppb	–	–	9	–	–	–	12	13	11	22	72	8	22	16	5	<5	<5	11
Au	–	6	3	–	–	7	–	4	–	–	–	–	–	–	–	–	–	–
Ir	–	6	6	–	–	2	–	5	–	–	–	–	–	–	–	–	–	–
Os	–	3	–	–	–	–	–	–	–	–	–	–	–	–	–	–	–	–
Pd	–	9	3	–	–	10	–	5	–	–	–	–	–	–	–	–	–	–
Pt	–	237	224	–	–	141	–	180	–	–	–	–	–	–	–	–	–	–
Rh	–	18	17	–	–	8	–	15	–	–	–	–	–	–	–	–	–	–
Ru	–	20	19	–	–	12	–	17	–	–	–	–	–	–	–	–	–	–
La ppm	133	196	182	140	146	118	139	155	192	173	186	148	177	153	169	209	204	159
Ce	421	1061	979	554	719	521	850	948	1271	1215	1120	728	1167	1032	739	993	1001	660
Pr	32.7	45.3	41.3	33.1	34.6	28.2	31.0	35.9	45.2	45.9	46.3	35.7	44.1	38.0	35.9	43.8	44.7	36.8
Nd	125	166	166	126	128	105	127	145	183	172	172	133	163	141	146	175	181	148
Sm	27.7	37.0	36.8	28.9	28.3	23.9	27.4	31.9	40.0	40.5	39.7	29.2	37.1	32.1	33.7	38.8	38.9	35.7
Eu	6.75	8.56	8.99	6.58	6.39	5.80	6.84	7.81	9.78	9.69	9.31	7.32	8.96	7.84	8.47	9.61	9.97	8.52
Gd	29.4	38.0	38.7	28.8	29.7	24.0	30.0	33.1	41.7	39.4	37.5	28.0	36.6	31.5	37.6	42.8	42.6	36.5
Tb	4.64	6.11	6.27	4.72	4.76	3.88	4.90	5.50	6.78	7.05	6.53	4.61	6.46	5.48	6.12	6.65	6.70	6.08
Dy	29.0	38.2	37.8	28.9	29.5	22.9	29.4	32.4	39.9	38.0	36.1	25.2	34.9	30.2	36.3	38.0	37.3	35.5
Y	128	147	144	132	128	93.4	124	121	146	149	147	105	152	130	171	154	142	159
Ho	5.96	7.53	7.86	6.18	5.97	4.75	6.01	6.76	8.30	8.16	7.84	5.31	7.72	6.69	7.50	7.74	7.68	7.23
Er	15.9	20.8	21.6	16.5	16.6	13.0	17.0	18.3	22.6	21.1	20.5	13.5	19.9	17.6	21.2	22.5	21.9	20.4
Tm	2.43	3.39	3.43	2.54	2.53	1.99	2.70	2.78	3.47	3.36	3.26	2.06	3.24	2.80	3.08	3.38	3.13	2.93
Yb	16.6	21.5	22.5	16.9	16.9	12.9	17.9	18.2	22.6	21.2	20.4	12.8	20.2	17.6	20.2	21.1	20.4	18.9
Lu	2.46	3.38	3.16	2.68	2.73	2.10	2.53	2.62	3.24	3.32	3.26	1.94	3.20	2.76	3.18	3.33	3.21	2.89
ΣREY ¹	979	1799	1699	1128	1299	982	1415	1564	2034	1947	1855	1280	1881	1649	1439	1769	1764	1339
%Heavy ²	24.6	16.4	17.3	21.8	18.7	18.8	17.0	15.9	14.9	15.4	15.7	16.1	15.6	15.3	21.9	17.5	16.7	22.3
Ce _{cn} ³	1.50	2.63	2.63	1.90	2.36	2.11	3.01	2.97	3.19	3.23	2.84	2.35	3.11	3.18	2.19	2.39	2.43	2.01
Ce _{sn} ³	1.47	2.60	2.61	1.88	2.33	2.08	2.99	2.93	3.15	3.14	2.78	2.31	3.05	3.12	2.19	2.39	2.42	1.99

Appendix 2

Table A2
Average contents for compiled data for nodules from the Cook Islands EEZ.

	This study		Compiled mean ¹	
	Mean	N	Mean	N
Fe wt.%	16.2	54	16.1	1158
Mn	16.9	54	16.1	1158
Si	8.03	54	7.30	209
Al	3.42	54	3.01	209
Mg	1.42	54	1.34	204
K	0.90	54	0.89	209
Ca	1.99	54	1.95	209
Na	1.76	54	1.84	209
Ti	1.28	54	1.20	74
As ppm	150	54	147	69
Co	3751	54	4113	1158
Cu	2309	54	2262	1158
Mo	295	54	295	79
Nb	91	54	90	67
Ni	3767	54	3805	1145
Pb	976	54	897	202
Th	36	54	37	67
U	9.5	54	10	67
V	504	54	508	61
W	59	54	64	67
Zn	492	54	545	222
Zr	555	54	524	75
ΣREY	1678	54	1665	59
Pt ppb	232	19	210	32

¹ Data from Japanese cruises in 1985, 1986, 1990, 2000 (JICA/MMAJ, 2001), n = 5 to 956; this study, n = 54, 19 for Pt; Landmesser et al. (1976), n = 13; Usui and Mita (1994), n = 135.

References

- Anders, E., Grevesse, N., 1989. Abundances of the elements: meteoritic and solar. *Geochim. Cosmochim. Acta* 53, 197–214.
- Bau, M., Schmidt, K., Koschinsky, A., Hein, J., Kuhn, T., Usui, A., 2014. Discriminating between different genetic types of marine ferro-manganese crusts and nodules based on rare earth elements and yttrium. *Chem. Geol.* 381, 1–9.
- Clark, A.L., Lum, J.A., Li, C., Icay, W., Morgan, C., Igarashi, Y., 1995. Economic and Development Potential of Manganese Nodules within the Cook Islands Exclusive Economic Zone (EEZ). The East-West Center, Honolulu, HI (34 pages).
- Cronan, D.A., 2006. Processes in the formation of central Pacific manganese nodule deposits. *J. Mar. Sci. Environ.* C4, 41–48.
- Cronan, D.A., 2013. The Distribution, Abundance, Composition and Resource Potential of the Manganese Nodules in the Cook Islands Exclusive Economic Zone. Cook Islands Seabed Minerals Authority, Report 1, May 2013, Rarotonga, Cook Islands.
- Cronan, D.S., Hodgkinson, R.A., Miller, S., 1991. Manganese nodules in the EEZ's of island countries in the southwestern equatorial Pacific. *Mar. Geol.* 98, 425–435.
- Cronan, D.S., Rothwell, G., Croudace, I., 2010. An ITRAX geochemical study of ferromanganese sediments from the Penrhyn Basin, South Pacific Ocean. *Mar. Georesour. Geotechnol.* 28, 207–221.
- Glasby, G.P., Keays, R.R., Rankin, P.C., 1978. The distribution of rare earth, precious metal and other trace elements in Recent and fossil deep-sea manganese nodules. *Geochim. J.* 12, 229–243.
- Hein, J.R., Koschinsky, A., 2014. Deep-ocean Ferromanganese Crusts and Nodules. In: Holland, H.D., Turekian, K.K. (Eds.), 2nd ed. Treatise on Geochemistry vol. 13. Elsevier, Oxford, pp. 273–291 (Chapter 11).
- Hein, J.R., Petersen, S., 2013. The Geology of Manganese Nodules. In: Baker, E., Beaudoin, Y. (Eds.), Secretariat of the Pacific Community, Deep Sea Minerals: Manganese Nodules, A Physical, Biological, Environmental, and Technical Review v. 1B. SPC, Suva, Fiji, pp. 7–18 (<http://grida.no/publications/deep-sea-minerals/>).
- Hein, J.R., Koschinsky, A., Bau, M., Manheim, F.T., Kang, J.-K., Roberts, L., 2000. Cobalt-rich Ferromanganese Crusts in the Pacific. In: Cronan, D.S. (Ed.), Handbook of Marine Mineral Deposits. CRC Press, Boca Raton, Florida, pp. 239–279.
- Hein, J.R., Mizell, K., Koschinsky, A., Conrad, T.A., 2013. Deep-ocean mineral deposits as a source of critical metals for high- and green-technology applications: comparison with land-based resources. *Ore Geol. Rev.* 51, 1–14.
- ISA, International Seabed Authority, 2010. A Geologic Model for Polymetallic Nodule Deposits in the Clarion–Clipperton Fracture Zone. Kingston, Jamaica: ISA Technical Study No. 6. (211 pp.)
- JICA/MMAJ, 2001. Report on the Cooperative Study Project of the Deep Sea Mineral Resources in Selected Offshore Area of the SOPAC Region, v. 1: Sea Area of the Cook Islands. Japan International Cooperation Agency and Metal Mining Agency of Japan (322 pages).
- Kingan, S.G., 1998. Manganese Nodules of the Cook Islands. SOPAC Miscellaneous Report 295. SOPAC Secretariat, Suva, Fiji (24 pages).
- Klovan, J.E., Imbrie, J., 1971. An algorithm and FORTRAN-IV program for large-scale Q-mode factor analysis and calculation of factor scores. *Math. Geol.* 3, 61–77.
- Landmesser, C.W., Kroenke, L.W., Glasby, G., Sawtell, G.H., Kingan, S., Utanga, E., Utanga, A., Cowan, G., 1976. Manganese Nodules from the South Penrhyn Basin, Southwest Pacific. South Pacific Marine Geological Notes 1 (3). CCOP-SOPAC Secretariat, Suva, Fiji, pp. 17–40.
- Malnic, J., 2008. A Frontier Advance in Processing Oxide Nickel Ores. Technical Paper for International Seabed Authority Workshop on Polymetallic Nodule Mining Technology—Current Status and Challenges Ahead. 18–22 February 2008, Chennai India.
- Manheim, F.T., Lane-Bostwick, C.M., 1988. Cobalt in ferromanganese crusts as a monitor of hydrothermal discharge on the sea floor. *Nature* 335, 59–62.
- McLennan, S.M., 1989. Rare earth elements in sedimentary rocks: influence of provenance and sedimentary processes. In: Lipen, B.R., McKay, G.A. (Eds.), Geochemistry and Mineralogy of Rare Earth Elements. Reviews in Mineralogy vol. 21. Mineralogical Society of America, Washington, D.C.
- Mudd, G.M., Weng, Z., Jowitt, S.M., Turnbull, I.D., Graedel, T.E., 2013. Quantifying the recoverable resources of by-product metals: the case of cobalt. *Ore Geol. Rev.* 55, 87–98.
- Okamoto, N., 2003. Summary Report on the Japan/SOPAC Cooperative Deep-sea Mineral Resources Study Programme, Four R/V Hakurei-Maru No. 2 Cruises, for Polymetallic Manganese Nodules, the EEZ of the Cook Islands. SOPAC Technical Report 359. SOPAC, Suva Fiji (59 pp.).
- Pisias, N.G., Murray, R.W., Scudder, R.P., 2013. Multivariate statistical analysis and partitioning of sedimentary geochemical data sets: general principles and specific MATLAB scripts. *Geochim. Geophys. Geosyst.* 14, 4015–4020. <http://dx.doi.org/10.1002/ggge.20247>.
- Sibson, R., 1981. A Brief Description of Natural Neighbor Interpolation. Chapter 2. Interpolating Multivariate Data. John Wiley & Sons, New York, pp. 21–36.
- U.S. Geological Survey, 2013. Mineral Commodity Summaries 2013. U.S. Geological Survey (198 p.).
- Usui, A., Mita, N., 1994. IX. Mineralogy, geochemistry and internal growth structure of manganese nodules in the western part of the Penrhyn Basin, South Pacific (GH83–3 Area). Geological Survey of Japan Cruise Report No. 23, pp. 165–185.
- Verlaan, P.A., Cronan, D.S., Morgan, C.L., 2004. A comparative analysis of compositional variations in and between marine ferromanganese nodules and crusts in the South Pacific and their environmental controls. *Prog. Oceanogr.* 63, 125–158.
- Yamazaki, T., 2008. Model Mining Units of the 20th Century and the Economics (Production Requirements, Area Requirements and Vertical Integration). Technical Paper for International Seabed Authority Workshop on Polymetallic Nodule Mining Technology—Current Status and Challenges Ahead. 18–22 February 2008, Chennai India.

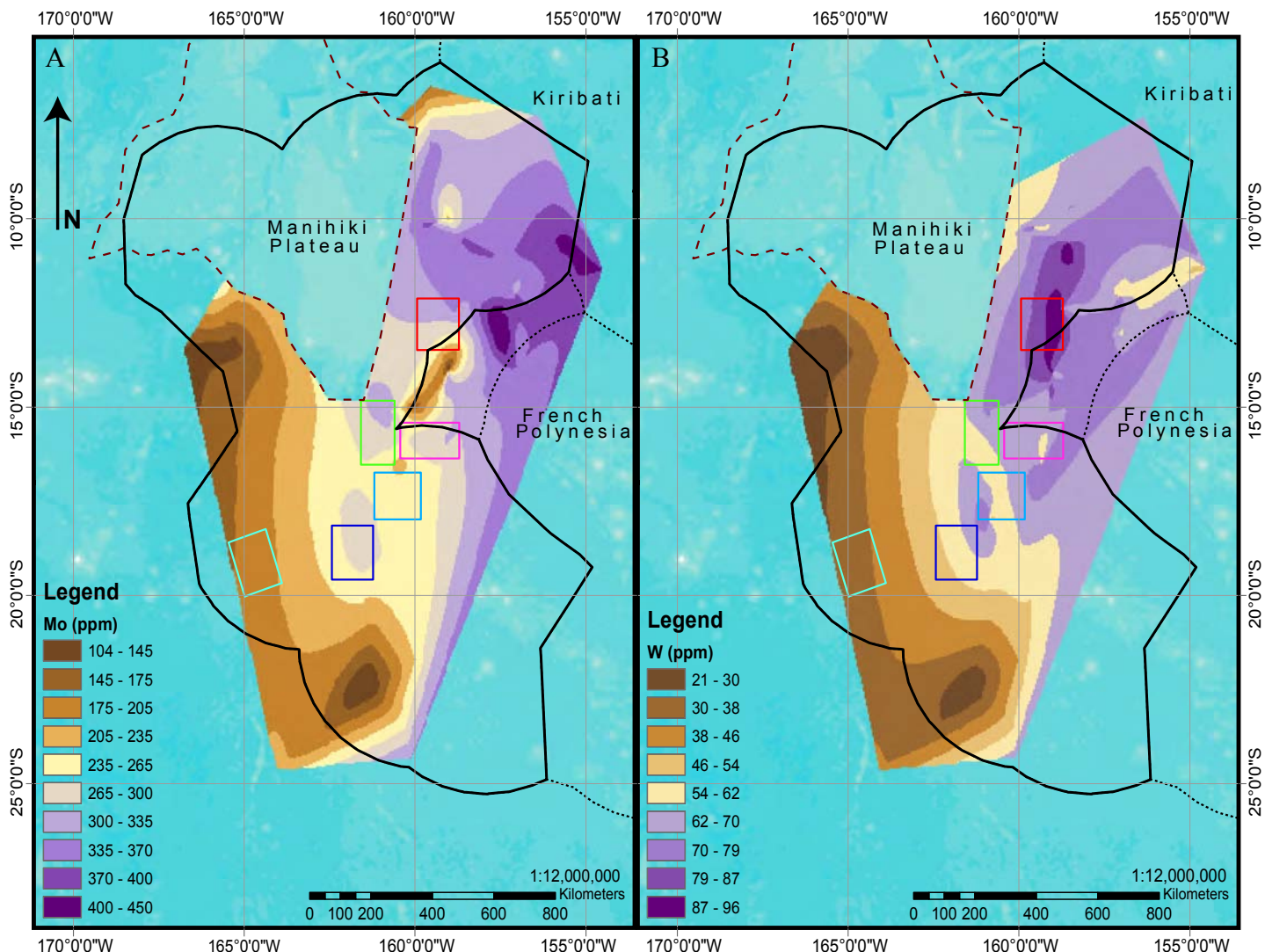


Fig. S.1. Metal concentration distribution maps for (A) Mo (ppm) and (B) W (ppm) from Cook Islands nodules; colored rectangles are labeled in Fig. 5, and data within each rectangle are quantified in Table 3

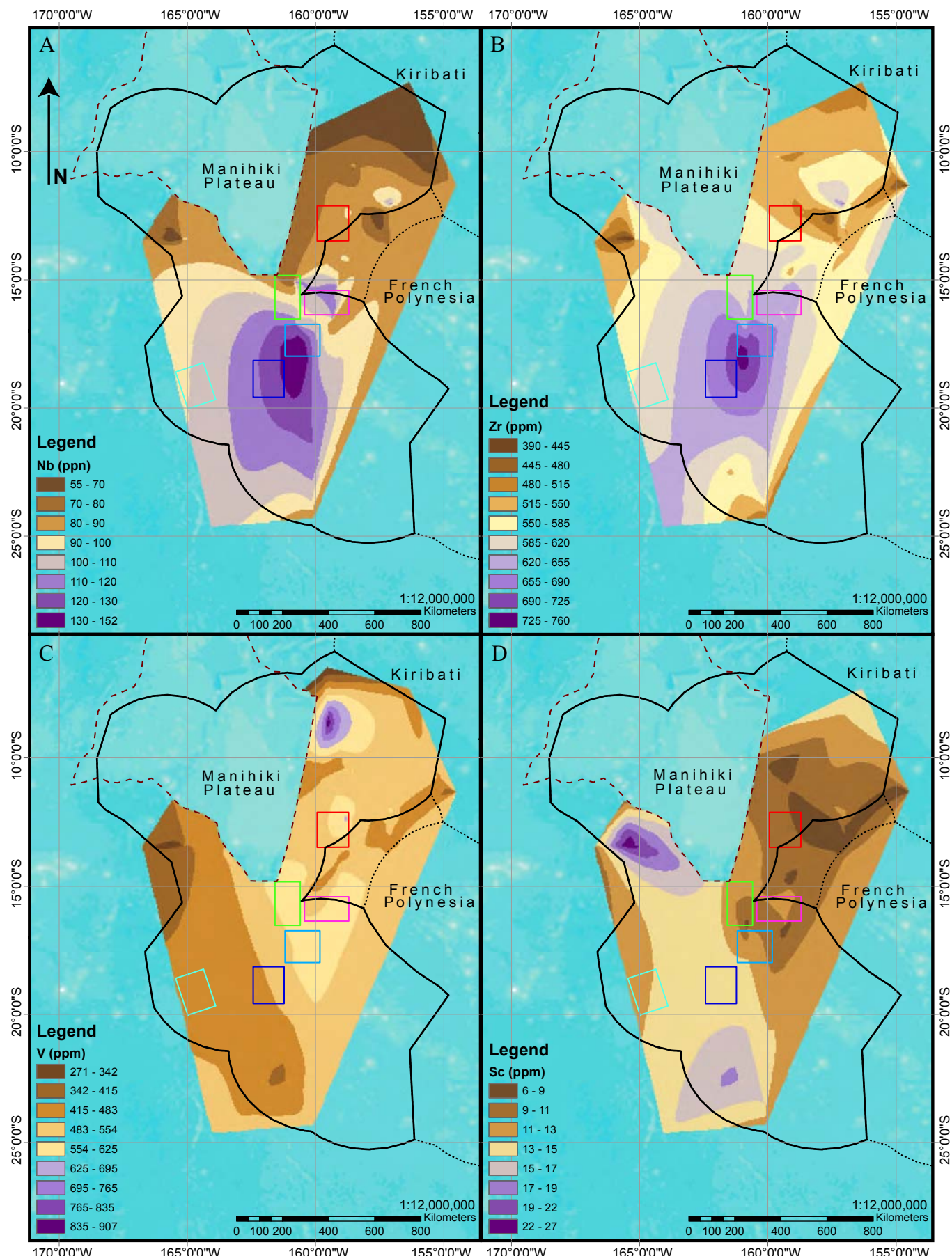


Fig. S.2. Metal concentration distribution maps for (A) Nb (ppm), (B) Zr (ppm), (C) V (ppm), and (D) Sc (ppm) from Cook Islands nodules; colored rectangles are labeled in Fig. 5, and data within each rectangle are quantified in Table 3

Table S.1. X-Ray diffraction mineralogy for manganese nodules, Cook Islands EEZ

Sample	Major	Moderate	Minor
1021-G991	$\delta\text{-MnO}_2$	Asbolane/buserite, Birnessite	Plagioclase, K-feldspar, Quartz, Phillipsite
1021-G995	$\delta\text{-MnO}_2$	--	Plagioclase, K-feldspar, Quartz, Asbolane/Buserite
1021-G1001	$\delta\text{-MnO}_2$	Pyroxene	Plagioclase, Buserite, Magnetite
1021-G1003	$\delta\text{-MnO}_2$	Asbolane	Goethite, Plagioclase, K-feldspar, Quartz, Phillipsite
1021-G1004	$\delta\text{-MnO}_2$	Asbolane/Buserite	Birnessite, Plagioclase, K-feldspar, Quartz
CK-76-1 STN-03-FFG-02A	$\delta\text{-MnO}_2$	--	Buserite, Phillipsite, Plagioclase, K-feldspar, Quartz
CK-76-1 STN-03-FFG-06A	$\delta\text{-MnO}_2$	--	Plagioclase, K-feldspar, Quartz
CK-76-1 STN-03-FFG-06B	$\delta\text{-MnO}_2$	Birnessite	Plagioclase, K-feldspar, Quartz
CK-76-1 STN-04-FFC-04	$\delta\text{-MnO}_2$	--	Plagioclase, Quartz
CK-76-1 STN-05-FFG-08A	$\delta\text{-MnO}_2$	--	Plagioclase, K-feldspar, Birnessite, Phillipsite, Asbolane, Quartz, Sepiolite?
CK-76-1 STN-05-FFG-08B	$\delta\text{-MnO}_2$	--	Plagioclase, Asbolane, Phillipsite, K-feldspar, Quartz
CK-76-1 STN-06-FFG-09	$\delta\text{-MnO}_2$	Plagioclase	K-feldspar, Quartz
CK-76-1 STN-07-FFG-10A	$\delta\text{-MnO}_2$	--	Plagioclase, K-feldspar, Birnessite, Quartz, Asbolane
CK-76-1 STN-07-FFG-10B	$\delta\text{-MnO}_2$	--	Plagioclase, Birnessite, Phillipsite, Quartz, K-feldspar
CK-76-1 STN-08-FFG-11	$\delta\text{-MnO}_2$	--	Plagioclase, K-feldspar, Quartz
CK-76-1 STN-10-FFG-13	$\delta\text{-MnO}_2$	Birnessite	Plagioclase, Quartz
CK-76-1 STN-11-FFG-14A	$\delta\text{-MnO}_2$	Birnessite	Plagioclase, K-feldspar, Quartz, Phillipsite?
CK-76-1 STN-11-FFG-14B	$\delta\text{-MnO}_2$	Birnessite	Plagioclase, Quartz, K-feldspar?, Phillipsite?
CK-76-1 STN-11-FFG-14C-MRT-B0-7	$\delta\text{-MnO}_2$	--	Plagioclase, K-feldspar, Birnessite, Phillipsite, Quartz
CK-76-1 STN-11-FFG-14C-MRU-B0-13	$\delta\text{-MnO}_2$	--	Plagioclase, K-feldspar, Phillipsite, Birnessite, Asbolane, Quartz
CK-76-1 STN-11-FFG-14C-MRU-L0-5	$\delta\text{-MnO}_2$	--	Plagioclase, K-feldspar, Birnessite, Pyroxene, Quartz
CK-76-1 STN-11-FFG-14C-MRU-L5-13	$\delta\text{-MnO}_2$	--	Birnessite and/or Phillipsite, Plagioclase, K-feldspar, Quartz
CK-76-1 STN-11-FFG-14D	$\delta\text{-MnO}_2$	--	Plagioclase, K-feldspar, Birnessite, Phillipsite, Asbolane, Quartz
CK-76-1 STN-12-FFG-15	$\delta\text{-MnO}_2$	--	Asbolane, Plagioclase, K-feldspar, Quartz, Smectite?
CK-78-2 STN-01-FFG-02A	$\delta\text{-MnO}_2$	Asbolane	Plagioclase, K-feldspar, Birnessite, Quartz
CK-78-2 STN-01-FFG-02B	$\delta\text{-MnO}_2$	--	Birnessite, Plagioclase, K-feldspar, Quartz, Phillipsite?
CK-78-2 STN-02-FFG-03A	$\delta\text{-MnO}_2$	Asbolane	Plagioclase, K-feldspar, Quartz
CK-78-2 STN-02-FFG-03A	$\delta\text{-MnO}_2$	Asbolane	Plagioclase, K-feldspar, Quartz
CK-78-2 STN-02-FFG-03B	$\delta\text{-MnO}_2$	Asbolane	K-feldspar, Plagioclase, Birnessite, Quartz
CK-78-2 STN-02-FFG-04	$\delta\text{-MnO}_2$	Asbolane	Plagioclase, K-feldspar, Quartz

Table S.1 continued

Sample	Major	Moderate	Minor
CK-78-2 STN-03-FFG-05	$\delta\text{-MnO}_2$	Asbolane	Plagioclase, K-feldspar, Quartz
CK-78-2 STN-03-FFG-06	$\delta\text{-MnO}_2$	--	Plagioclase, Asbolane, Phillipsite, K-feldspar, Quartz
CK-78-2 STN-04-FFG-07	$\delta\text{-MnO}_2$	--	Birnessite, Phillipsite, Plagioclase, K-feldspar, Quartz, Smectite?
CK-78-2 STN-04-FFG-08	$\delta\text{-MnO}_2$	Asbolane	Phillipsite, Plagioclase, K-feldspar, Quartz, Birnessite
CK-78-2 STN-05-FFG-09A	$\delta\text{-MnO}_2$	--	Birnessite, Plagioclase, K-feldspar, Quartz
CK-78-2 STN-05-FFG-09B	$\delta\text{-MnO}_2$	--	Asbolane, Plagioclase, Phillipsite, K-feldspar, Quartz
CK-78-2 STN-05-FFG-10	$\delta\text{-MnO}_2$	--	Plagioclase, Phillipsite, Asbolane, Quartz, K-feldspar
CK-78-2 STN-07-FFG-13A	$\delta\text{-MnO}_2$	--	Birnessite, Plagioclase, K-feldspar, Phillipsite, Quartz, Goethite?
CK-78-2 STN-07-FFG-13B	$\delta\text{-MnO}_2$	--	Nontronite, Plagioclase, K-feldspar, Quartz
CK-78-2 STN-07-FFG-14A	$\delta\text{-MnO}_2$	Asbolane	K-feldspar, Plagioclase, Nontronite, Quartz
CK-78-2 STN-07-FFG-14B	$\delta\text{-MnO}_2$	--	Nontronite, Plagioclase, K-feldspar, Quartz
CK-78-2 STN-08-FFG-15B	$\delta\text{-MnO}_2$	Plagioclase, K-feldspar, Phillipsite	Asbolane, Pyroxene, Birnessite, Quartz
CK-78-2 STN-08-FFG-16	$\delta\text{-MnO}_2$	Asbolane, Phillipsite	Plagioclase, K-feldspar, Quartz
CK-80-1 STN-03 WGCM-03	$\delta\text{-MnO}_2$	Birnessite	Phillipsite, Plagioclase, Illite, Quartz
CK-80-1 STN-03-WGCM-13	$\delta\text{-MnO}_2$	--	K-feldspar, Plagioclase, Phillipsite, Asbolane, Birnessite, Quartz
CK-80-1 STN-04 WGCM-04A	$\delta\text{-MnO}_2$	Asbolane	Birnessite, Phillipsite, Plagioclase, Quartz
CK-80-1 STN-04 WGCM-04B	$\delta\text{-MnO}_2$	Asbolane	Birnessite, Phillipsite, Plagioclase, K-feldspar, Quartz
CK-80-1 STN-10 WGCM-08	$\delta\text{-MnO}_2$, Asbolane	Birnessite, Phillipsite	Plagioclase, K-feldspar, Quartz
CK-80-2 STN-17-WG-01A	$\delta\text{-MnO}_2$	--	Plagioclase, K-feldspar, Asbolane, Phillipsite, Quartz
CK-80-2 STN-17-WG-1B-MRT-B0-8	$\delta\text{-MnO}_2$	--	Plagioclase, Birnessite, Phillipsite, Asbolane, Quartz, K-feldspar
CK-80-2 STN-17-WG-1B-MRU-B0-11	$\delta\text{-MnO}_2$	--	Plagioclase, K-feldspar, Phillipsite, Quartz, Sepiolite?
U321A	$\delta\text{-MnO}_2$	Phillipsite	Plagioclase, K-feldspar, Buserite/Asbolane, Birnessite, Quartz
U339 <20mm	$\delta\text{-MnO}_2$	--	Birnessite, Plagioclase, Phillipsite, K-feldspar, Quartz, Sepiolite
U339 >20mm	$\delta\text{-MnO}_2$	--	Phillipsite, Plagioclase, K-feldspar, Buserite, Quartz
U340	$\delta\text{-MnO}_2$	Phillipsite	Plagioclase, K-feldspar, Asbolane/Buserite, Quartz

Major = >25%, Moderate = 5-25%, Minor = <5%; ? means content too low to be certain of identification

Supplementary Material

Equations for total abundance area and tonnage of nodules:

$$1. A_0 = \sum \frac{(S_0)^2 C_0}{10^6}$$

$$2. T_0 = \sum \frac{(S_0)^2 C_0 V_0}{10^6}$$

Where A_0 is the area of the distribution map contained within the Cook Islands' EEZ, but excluding Manihiki Plateau. T_0 is tonnage of nodules within the distribution map and confined to the Cook Islands' EEZ, but excluding the Manihiki plateau. S_0 is the default cell size in meters assigned to the distribution map ($x=y$), V_0 is the given value (g/m^2), and C_0 the number of cells with said value.

Equations for element tonnages within a potential mine site:

$$1. A_m = \sum \frac{(S_m)^2 C_m}{10^6}$$

$$2. W_m = \sum \frac{(S_m)^2 C_m V_m}{10^3}$$

$$3. A_c = \frac{(S_c)^2 C_c}{10^6}$$

$$4. A_{cm} = \frac{A_c}{A_m}$$

$$5. W_c = A_{cm} W_m$$

$$6. W_e = \frac{V_c W_c}{10^6}$$

$$7. T_c = \sum \frac{W_e}{1000}$$

Where A_m is the total km^2 of the potential mine site. S_m is the cell size, where x and y are measured in m and $x=y$, based on the abundance map within the site. V_m is the specified abundance value in g/m^2 . C_m is the number of cells with said specified value. W_m is the total weight (kg_{wet}) of nodules contained within the site. A_c is the area of a cell at a specific element concentration. S_c is the assigned default cell size measured in m and $x=y$, based on the element concentration distribution map created in ArcGIS_10.2. V_c is the specified ppm concentration of an element, while C_c is the number of cells with said concentration. W_c is the weight of nodules (kg_{wet}) at said concentration. A_{cm} is the ratio of cell area to total area in potential mine site. W_e is the weight (kg_{wet}) of an element at specific concentration value. T_c is the total wet tones of an element contained with in the potential mine site.



Corrigendum

Corrigendum to “Critical metals in manganese nodules from the Cook Islands EEZ, abundances and distributions” [Ore Geol. Rev. 68 (2015) 97–116]



James R. Hein ^{a,*}, Francesca Spinardi ^a, Nobuyuki Okamoto ^b, Kira Mizell ^a, Darryl Thorburn ^c, Akuila Tawake ^d

^a U.S. Geological Survey, PCMSC, 400 Natural Bridges Dr., Santa Cruz, CA 95060, USA

^b Sea-Floor Mineral Resources R&D Division, Metals Mining Technology Dept., JOGMEC, 2-10-1 Toranomon, Minato-ku, Tokyo 105-0001, Japan

^c Seabed Minerals Authority, Avarua, Rarotonga, Cook Islands

^d SOPAC Division of the SPC, Private Mail Bag, GPO, Suva, Fiji

Dear Journal Manager and Editor,

The authors regret to report that mistakes were found in the article after its availability online. The following problems happened to our article, and we would kindly ask you to correct the found mistakes.

- (1) Appendix 1, **Table A.1** “Hygroscopic water-normalized (0% H₂O⁻) chemical composition of Cook Islands EEZ manganese nodules”. In this table, the element concentrations of V and W have been switched intermittently throughout; low Cl concentrations due to dilution error are corrected.

Table A.1

Hygroscopic water-normalized (0% H₂O⁻) chemical composition of Cook Islands EEZ manganese nodules.

	CK-76-1 STN-03 FFC-02A	CK-76-1 STN-03 FFG-06A	CK-76-1 STN-03 FFG-06B	CK-76-1 STN-04 FFG-04	CK-76-1 STN-05 FFG-08A	CK-76-1 STN-05 FFG-08B	CK-7-16 STN-06 FFG-09	CK-76-1 STN-07 FFG-10A	CK-76-1 STN-07 FFG-10B	CK-76-1 STN-08 FFG-11	CK-76-1 STN-10 FFG-13	CK-76-1 STN-11 FFG-14A
Sample Type Description	Nodule B-1:29 ^d	Nodule B-1:35	Nodule B-3:22–25	Nodule B-1:27	Nodule B-1:40	Nodule B-2:16–23	Nodule B-4:22–28	Nodule B-2:24–29	Nodule B-0.13:43	Nodule B-1:47	Nodule B-1:35	Nodule B-1:30
Fe wt%	19.6	19.7	20.4	19.4	17.0	16.6	17.4	16.9	16.3	17.4	19.4	21.1
Mn	15.6	17.9	16.8	17.7	17.8	17.4	17.9	18.2	18.4	20.4	17.9	16.8
Fe/Mn	1.26	1.10	1.21	1.10	0.96	0.95	0.97	0.93	0.88	0.85	1.08	1.26
Si	6.69	7.16	7.19	7.03	5.87	6.86	7.78	6.42	6.47	6.70	6.65	7.32
Al	2.79	3.09	3.13	3.11	2.49	3.01	3.50	2.93	2.57	2.81	2.84	2.98
Mg	1.16	1.26	1.33	1.31	1.15	1.27	1.38	1.29	1.18	1.22	1.25	1.27
K	0.60	0.71	0.68	0.64	0.59	0.63	0.81	0.64	0.72	0.70	0.72	0.70
Ca	1.93	2.11	2.04	2.03	1.91	2.16	2.09	1.90	1.98	2.20	2.02	2.13
Na	1.61	1.84	1.80	1.76	1.62	1.61	1.86	1.63	1.67	1.90	1.78	1.84
P	0.35	0.37	0.38	0.36	0.31	0.43	0.38	0.33	0.31	0.35	0.38	0.41
Ti	1.72	1.76	1.86	1.70	1.29	1.40	1.47	1.24	1.14	1.17	1.57	1.80
LOI	26.6	30.7	30.1	30.1	30.4	27.7	30.1	27.7	30.3	31.7	31.6	28.8
H ₂ O ⁻	9.90	20.3	19.4	18.2	10.8	10.1	17.7	10.5	11.8	19.7	19.2	18.2
H ₂ O ⁺	14.8	7.50	8.60	8.60	18.2	15.6	8.60	15.5	17.4	8.30	8.10	7.90
Ag ppm	0.18	0.30	0.33	0.33	0.13	0.18	0.30	0.18	0.15	0.29	0.33	0.32
As	180	161	165	164	163	147	145	172	178	171	172	172
Ba	1210	1368	1290	1357	1300	1224	1187	1080	1644	1357	1423	1296
Be	4.2	3.6	3.7	4.2	4.3	4.0	3.4	3.6	4.8	4.0	4.3	4.3
Bi	14	14	15	13	13	12	11	13	15	14	14	15
Cd	3.5	3.3	3.5	3.9	3.8	5.0	4.3	4.6	4.1	3.8	3.7	3.3
Cl	6445	7829	7630	7176	6550	5847	7108	6497	6731	7808	7079	8178

(continued on next page)

DOI of original article: <http://dx.doi.org/10.1016/j.oregeorev.2014.12.011>

* Corresponding author.

E-mail address: jhein@usgs.gov (J.R. Hein).

Table A.1 (continued)

Sample Type Description	CK-76-1 STN-03 FFC-02A	CK-76-1 STN-03 FFG-06A	CK-76-1 STN-03 Nodule B-1:29 ⁴	CK-76-1 STN-04 FFG-04	CK-76-1 STN-05 FFG-08A	CK-76-1 STN-06 FFG-08B	CK-7-16 STN-07 FFG-09	CK-76-1 STN-07 FFG-10A	CK-76-1 STN-07 FFG-10B	CK-76-1 STN-08 FFG-11	CK-76-1 STN-10 FFG-13	CK-76-1 STN-11 FFG-14A
	Nodule B-1:35	Nodule B-3:22-25	Nodule B-1:27	Nodule B-1:40	Nodule B-2:16-23	Nodule B-4:22-28	Nodule B-4:22-28	Nodule B-2:24-29	Nodule B-0.13:43	Nodule B-1:47	Nodule B-1:35	Nodule B-1:30
Co	4473	4956	4529	4694	4608	3949	3827	4480	5408	4869	5173	4866
Cr	18	29	26	23	4.5	20	23	6.7	11	17	20	32
Cs	0.22	0.38	0.37	0.37	0.22	0.22	0.36	0.22	0.23	0.37	0.37	0.49
Cu	1243	1443	1613	1834	1570	2214	2260	1888	1712	1818	1572	1333
Ga	5.9	9.4	9.7	10	6.1	7.8	9.8	6.7	6.8	10	9.8	9.2
Hf	16	14	16	16	12	12	15	13	11	11	15	16
In	0.94	0.99	1.0	0.97	0.93	0.83	0.80	0.84	1.1	0.90	1.1	1.1
Li	22	21	26	32	25	40	41	34	28	22	26	20
Mo	238	300	251	293	277	255	286	292	359	390	323	249
Nb	112	110	124	119	90	90	101	95	93	83	114	125
Ni	2020	2723	2742	3227	2960	3526	3840	3229	3152	3362	3082	2482
Pb	1354	1197	1278	1198	1188	1110	959	1229	1293	1161	1287	1345
Rb	8.5	11	11	10	7.8	7.9	13	8.2	11	11	12	12
S	1554	2384	2233	2200	1570	1446	2187	1564	1927	2864	2351	2323
Sb	39	35	37	36	36	35	32	37	40	33	38	42
Sc	9.1	12	12	12	8.0	8.2	12	7.9	9.4	12	13	14
Se	0.89	1.0	0.99	0.98	0.45	0.67	0.73	0.89	0.34	0.75	0.62	0.98
Sn	11	7.3	6.8	6.7	6.2	7.6	5.6	12	11	6.0	6.4	7.0
Sr	1000	1080	1066	1062	983	960	991	951	1179	1199	1105	1084
Ta	3.9	3.6	3.7	3.2	2.8	2.8	2.4	2.4	2.9	2.0	1.9	3.2
Te	35	36	31	32	37	29	25	30	41	33	34	33
Th	55	51	52	45	39	31	30	39	40	38	59	64
Tl	141	130	125	150	198	199	149	193	235	169	137	112
U	13	11	11	11	12	11	10	12	12	11	11	11
V	608	600	587	615	575	515	535	568	654	574	624	594
W	58	65	53	64	80	61	57	68	98	80	69	56
Zn	446	479	504	490	433	494	495	432	518	469	490	467
Zr	603	595	658	637	496	523	611	522	500	545	613	675
Hg ppb	117	–	–	–	47	47	–	49	85	–	–	–
Au	–	9	–	–	6	–	9	–	4	6	7	–
Ir	–	6	–	–	6	–	5	–	6	6	6	–
Os	–	3	–	–	–	–	2	–	–	1	2	–
Pd	–	10	–	–	5	–	11	–	5	7	11	–
Pt	–	211	–	–	242	–	196	–	327	214	205	–
Rh	–	16	–	–	21	–	15	–	27	17	17	–
Ru	–	23	–	–	20	–	17	–	18	20	20	–
La ppm	188	213	207	207	167	151	180	156	173	199	230	221
Ce	1321	1481	1390	1320	1155	907	984	989	1315	1245	1510	1504
Pr	44.6	51.4	50.5	49.5	38.3	34.3	43.7	36.1	40.0	48.3	55.8	55.0
Nd	193	189	186	183	166	148	160	159	172	178	209	203
Sm	38.2	43.4	41.7	42.1	32.4	28.1	35.8	30.5	33.9	40.2	46.4	44.1
Eu	9.89	10.4	10.0	10.1	8.30	7.58	8.82	7.98	8.49	9.78	10.8	10.7
Gd	39.7	43.8	42.8	41.1	34.6	31.3	38.2	33.0	35.9	41.0	45.2	43.9
Tb	7.06	7.69	7.48	7.47	6.15	5.57	6.52	5.73	6.11	7.25	7.90	7.78
Dy	39.5	41.9	40.9	40.6	34.1	30.6	36.6	31.7	34.9	40.3	42.5	43.9
Y	149	163	161	158	132	131	162	134	141	156	171	167
Ho	7.90	8.62	8.51	8.42	7.03	6.52	7.78	6.60	7.22	8.28	8.81	8.67
Er	20.4	22.8	22.5	21.9	17.8	16.9	20.4	17.4	18.8	22.7	22.8	22.7
Tm	3.17	3.76	3.60	3.57	2.87	2.74	3.41	2.84	3.04	3.61	3.85	3.73
Yb	22.4	23.3	23.7	23.0	20.3	19.0	21.7	19.6	20.7	23.0	23.8	23.0
Lu	3.11	3.61	3.60	3.57	2.89	2.67	3.27	2.69	2.89	3.80	3.65	3.57
%REY ¹	2086	2307	2199	2119	1825	1522	1712	1632	2014	2027	2391	2362
%Heavy ²	14.5	14.3	14.7	15.0	14.6	16.7	18.0	16.0	13.8	15.6	14.2	14.2
Ce _{cn} ³	3.38	3.31	3.19	3.06	3.36	2.93	2.60	3.07	3.68	2.98	3.13	3.21
Ce _{sn} ³	3.33	3.26	3.13	3.01	3.33	2.91	2.56	3.04	3.64	2.93	3.07	3.14
Sample Type Description	CK-76-1 STN-11 FFG-14B	CK-76-1 STN-11 FFG-14C-MRT-B0-7	CK-76-1 STN-11 FFG-14C-MRU-B0-13	CK-76-1 STN-11 FFG-14C-MRU-L0-5	CK-76-1 STN-11 FFG-14C-MRU-L5-13	CK-76-1 STN-11 FFG-14D	CK-76-1 STN-12 FFG-14D					
	Nodule B-1:25	PC Nod B:0-7	PC Nod B:0-13	PC Nod L:0-5	PC Nod L:5-13	Node B-2:27-22	Node B-12:10-25					
Fe wt%	20.6	17.4	20.2	22.0	19.1	19.8	20.4					
Mn	16.3	14.3	15.1	14.5	15.3	15.6	16.1					
Fe/Mn	1.27	1.22	1.33	1.52	1.25	1.28	1.27					
Si	7.14	7.68	6.16	5.50	6.98	6.85	7.37					
Al	2.83	3.14	2.20	1.63	2.60	2.79	3.09					
Mg	1.24	1.09	1.09	1.00	1.02	1.20	1.45					
K	0.69	0.79	0.55	0.43	0.74	0.67	0.70					
Ca	2.06	2.11	1.94	1.84	1.90	1.96	1.92					

Table A.1 (continued)

Sample Type Description	CK-76-1 STN-11 FFG-14B Nodule B-1:25	CK-76-1 STN-11 FFG-14C-MRT-B0-7 PC Nod B:0-7	CK-76-1 STN-11 FFG-14C-MRU-B0-13 PC Nod B:0-13	CK-76-1 STN-11 FFG-14C-MRU-L0-5 PC Nod L:0-5	CK-76-1 STN-11 FFG-14C-MRU-L5-13 PC Nod L:5-13	CK-76-1 STN-11 FFG-14D Nodule B-2:27-22	CK-76-1 STN-12 FFG-15 Nodule B-12:10-25
Na	1.77	1.81	1.71	1.57	1.90	1.70	1.74
P	0.38	0.35	0.37	0.41	0.36	0.37	0.36
Ti	1.79	1.63	1.55	1.57	1.43	1.69	1.95
LOI	29.7	28.8	29.9	27.5	29.1	27.6	28.6
H ₂ O ⁻	18.1	10.5	11.9	7.40	12.2	11.9	17.5
H ₂ O ⁺	8.00	17.2	18.4	16.4	18.0	16.3	8.50
Ag ppm	0.38	0.12	0.17	0.13	0.21	0.16	0.36
As	177	145	209	185	247	176	170
Ba	1294	1263	1237	1231	1298	1192	1321
Be	4.3	4.6	4.4	4.3	4.6	4.2	4.1
Bi	15	11	16	15	18	15	15
Cd	3.5	2.9	2.8	2.5	2.5	3.4	3.7
Cl	7387	7572	8424	8473	8297	6880	7467
Co	4835	3642	4813	3877	4442	4449	4824
Cr	35	28	20	14	17	23	32
Cs	0.37	0.22	0.23	0.22	0.23	0.34	0.48
Cu	1343	1486	1079	685	994	1317	1867
Ga	9.2	5.5	5.4	3.9	3.6	5.8	10
Hf	17	10	16	13	21	17	18
In	1.1	0.87	1.1	1.3	1.1	1.1	1.1
Li	18	13	10	5.4	8.0	19	36
Mo	249	230	272	281	245	241	239
Nb	127	69	115	91	129	119	154
Ni	2527	1877	1691	1695	1720	2406	3188
Pb	1355	1094	1510	1339	1948	1396	1358
Rb	11	10	7.9	8.9	6.6	9.1	13
S	2198	1564	1589	1512	1595	1476	2061
Sb	43	31	47	38	48	44	45
Sc	14	9.6	9.2	8.1	7.9	9.2	14
Se	1.2	0.56	0.91	0.86	0.68	0.91	0.73
Sn	7.0	15	12	7.5	28	7.4	13
Sr	1089	943	1023	1078	1008	1019	1017
Ta	3.2	3.3	3.1	3.0	4.2	3.3	3.8
Te	32	27	36	31	32	34	30
Th	63	34	72	53	91	60	69
Tl	121	168	121	110	134	143	106
U	11	12	13	13	15	12	10
V	601	522	659	609	650	583	608
W	60	53	64	72	57	56	53
Zn	487	413	411	404	390	455	509
Zr	678	446	620	544	703	614	724
Hg ppb	—	57	58	94	18	50	—
Au	—	2	—	—	—	—	7
Ir	—	5	—	—	5	—	6
Os	—	—	—	—	—	—	2
Pd	—	5	—	—	2	—	6
Pt	—	146	—	—	148	—	232
Rh	—	14	—	—	16	—	17
Ru	—	18	—	—	16	—	19
La ppm	223	169	215	205	298	190	213
Ce	1502	962	1464	1307	1993	1283	1491
Pr	55.3	40.3	52.0	50.5	74.7	44.3	51.4
Nd	204	173	226	218	323	191	189
Sm	44.7	34.4	43.6	42.9	63.9	36.9	41.9
Eu	10.8	8.94	11.3	11.0	16.5	9.61	10.1
Gd	45.7	36.5	44.8	44.5	65.4	38.7	41.7
Tb	8.13	6.55	7.99	7.84	11.4	6.99	7.09
Dy	44.0	36.3	43.5	43.4	62.4	37.7	38.8
Y	170	144	157	158	212	149	145
Ho	8.82	7.45	8.63	8.76	12.0	7.60	7.55
Er	22.8	19.1	21.9	22.1	29.8	19.8	20.5
Tm	3.58	3.04	3.43	3.56	4.68	3.11	3.30
Yb	23.2	21.8	23.7	25.1	32.5	22.1	21.2
Lu	3.63	2.94	3.35	3.44	4.46	3.11	3.30

(continued on next page)

Table A.1 (continued)

	CK-76-1 STN-11 FFG-14B	CK-76-1 STN-11 FFG-14C-MRT-B0-7	CK-76-1 STN-11 FFG-14C-MRU-B0-13	CK-76-1 STN-11 FFG-14C-MRU-L0-5	CK-76-1 STN-11 FFG-14C-MRU-L5-13	CK-76-1 STN-11 FFG-14D	CK-76-1 STN-12 FFG-15
Sample Type Description	Nodule B-1:25	PC Nod B:0-7	PC Nod B:0-13	PC Nod L:0-5	PC Nod L:5-13	Nodule B-2:27-22	Nodule B-12:10-25
ΣREY^1	2370	1665	2326	2151	3205	2041	2286
%Heavy ²	14.4	17.2	14.0	15.2	14.1	14.6	13.1
Ce _{en} ³	3.18	2.73	3.25	3.02	3.14	3.27	3.34
Ce _{sn} ³	3.12	2.69	3.20	2.96	3.08	3.23	3.28
CK-78-2 STN-01 FFG-02A	CK-78-2 STN-01 FFG-02B	CK-78-2 STN-02 FFG-03	CK-78-2 STN-02 FFG-03B	CK-78 FFG-04	CK-78-2 STN-03 FFG-05	CK-78-2 STN-03 FFG-06	CK-78-2 STN-04 FFG-07
Sample Type Description	Nodules B-7:10-21	Nodules B-1/4:60	Nodules B-8:10-18	Nodules B-5:28-11	Nodule B-~6:Un	Nodule B-4:33-16	Nodule B-5:16-29
CK-78-2 STN-04 FFG-08	CK-78-2 STN-04 FFG-09A	CK-78-2 STN-05 FFG-09B	CK-78-2 STN-05 FFG-10	CK-78-2 STN-06 FFG-11	CK-78-2 STN-06 FFG-12	CK-78-2 STN-07 FFG-13	CK-78-2 STN-07 FFG-14
CK-78-2 STN-08 FFG-15	CK-78-2 STN-08 FFG-16	CK-78-2 STN-09 FFG-17	CK-78-2 STN-09 FFG-18	CK-78-2 STN-10 FFG-19	CK-78-2 STN-10 FFG-20	CK-78-2 STN-11 FFG-21	CK-78-2 STN-11 FFG-22
Fe wt%	14.7	15.2	14.0	13.6	12.9	16.1	13.9
Mn	21.1	19.6	22.3	19.8	23.9	20.9	19.4
Fe/Mn	0.70	0.78	0.63	0.69	0.54	0.77	0.71
Si	7.07	8.22	6.34	5.96	6.45	6.52	6.07
Al	3.49	3.30	3.30	2.97	3.45	3.08	3.09
Mg	1.57	1.31	1.80	1.60	2.07	1.44	1.59
K	0.76	0.91	0.73	0.63	0.74	0.73	0.69
Ca	2.18	2.17	2.24	1.97	2.12	2.20	2.16
Na	1.88	2.01	1.80	1.64	1.83	1.82	1.66
P	0.35	0.33	0.39	0.32	0.32	0.38	0.44
Ti	1.14	1.05	1.07	1.01	0.98	1.18	1.05
LOI	28.7	30.9	26.7	27.9	27.8	31.1	26.8
H ₂ O ⁻	16.7	18.7	13.7	6.60	15.9	19.0	6.80
H ₂ O ⁺	8.60	7.70	8.80	15.3	8.30	7.20	14.8
Ag ppm	0.26	0.26	0.25	0.16	0.19	0.36	0.10
As	131	134	131	133	118	154	124
Ba	1297	1378	1251	1124	1272	1370	1031
Be	3.4	3.9	3.0	3.4	2.6	4.4	3.2
Bi	11	13	9.9	8.9	8.2	12	8.9
Cd	6.2	4.2	7.1	6.9	8.6	5.4	6.7
Cl	6867	8155	6014	5790	5826	6963	6063
Co	3806	4034	3407	3597	2794	4111	3369
Cr	19	17	19	36	21	21	14
Cs	0.36	0.37	0.35	0.21	0.36	<0.1	0.21
Cu	3445	2571	4137	3458	5113	3086	3208
Ga	12	10	13	9.2	15	12	8.3
Hf	12	11	12	13	9.5	12	14
In	0.67	0.98	0.54	0.49	0.48	0.77	0.55
Li	80	33	107	90	134	51	77
Mo	373	370	417	391	449	374	355
Nb	84	84	83	76	73	89	83
Ni	5654	4071	6941	4593	8537	5173	4324
Pb	866	847	899	806	751	856	770
Rb	11	14	11	8.5	11	12	8.6
S	2881	2460	2317	1713	2259	2469	1609
Sb	36	36	35	35	36	37	35
Sc	11	12	10	6.7	9.0	11	6.5
Se	0.48	<0.2	0.70	0.86	0.71	0.99	0.86
Sn	4.6	5.5	5.7	7.5	4.6	21	3.0
Sr	1023	1005	970	905	898	1062	817
Ta	1.7	1.8	1.4	1.5	1.3	1.9	1.3
Te	21	34	17	17	14	24	19
Th	19	21	19	18	15	24	18
Tl	166	173	181	173	184	184	182
U	9.5	8.6	9.5	9.6	8.4	10	9.5
V	490	520	492	439	473	538	425
W	72	76	76	77	80	70	60
Zn	711	481	637	551	721	567	520
Zr	561	528	561	496	510	612	515
Hg ppb	—	—	—	19	—	15	—
Au	—	6	5	—	5	—	—
Ir	—	5	6	—	6	—	—
Os	—	1	1	—	2	—	—
Pd	—	7	6	—	6	—	—
Pt	—	284	307	—	328	—	—
Rh	—	17	21	—	24	—	—
Ru	—	20	19	—	19	—	—
La ppm	160	165	161	147	140	194	155
Ce	778	1065	703	651	583	930	661

Table A.1 (continued)

	CK-78-2 STN-01 FFG-02A	CK-78-2 STN-01 FFG-02B	CK-78-2 STN-02 FFG-03	CK-78-2 STN-02 FFG-03B	CK-78 FFG-04	CK-78-2 STN-03 FFG-05	CK-78-2 STN-03 FFG-06	CK-78-2 STN-04 FFG-07	CK-78-2 STN-04 FFG-08	CK-78-2 STN-05 FFG-09A	CK-78-2 STN-05 FFG-09B	CK-78-2 STN-05 FFG-10	
Sample Type Description	Nodules B-7:10-21	Nodules B-1/4:60	Nodules B-8:10-18	Nodules B-5:28-11	Nodule B-8:19-25	Nodule B~6:Un	Nodule B-4:33-16	Nodule B-5:16-29	Nodule B-7:29-10	Nodule B-1:65	Nodule B-4:23-28	Nodule B~4:Un	
Pr	36.3	39.4	37.4	32.4	32.2	43.0	33.5	36.2	31.1	43.6	47.6	36.6	
Nd	136	144	140	132	122	159	137	137	128	162	176	149	
Sm	29.9	32.3	30.6	28.4	27.5	34.7	29.3	30.4	27.9	35.2	38.4	32.0	
Eu	7.64	7.58	7.91	7.27	6.59	8.57	7.67	7.64	7.22	7.98	8.69	8.06	
Gd	32.2	33.5	33.6	31.4	30.1	39.3	33.6	31.8	32.0	36.0	39.7	33.8	
Tb	5.65	5.78	5.79	5.15	5.12	6.21	5.38	5.25	5.10	5.85	6.12	5.56	
Dy	32.2	32.3	34.6	31.3	29.0	37.7	32.7	32.8	30.8	35.0	38.2	32.4	
Y	144	145	146	127	130	157	135	140	129	150	160	125	
Ho	6.94	7.07	7.16	6.53	6.11	7.77	6.73	6.82	6.52	7.35	7.62	6.64	
Er	18.6	18.9	19.0	17.9	16.6	20.9	18.8	18.2	17.8	19.8	20.5	17.6	
Tm	3.18	3.05	3.17	2.78	2.84	3.48	2.96	2.83	2.77	3.09	3.13	2.78	
Yb	20.0	19.8	20.3	18.7	17.2	22.6	19.2	18.5	18.0	20.2	20.5	17.7	
Lu	3.09	3.15	3.34	2.63	2.77	3.47	2.74	2.87	2.53	3.07	3.20	2.53	
ΣREY^1	1413	1722	1354	1241	1151	1667	1281	1156	1052	1876	1838	1486	
%Heavy ²	19.4	16.0	20.8	20.2	21.4	18.4	20.7	23.1	23.9	15.4	16.7	16.9	
Ce _{cn} ³	2.38	3.10	2.12	2.19	2.02	2.37	2.13	1.64	1.64	2.90	2.47	2.56	
Ce _{sn} ³	2.36	3.05	2.09	2.18	2.00	2.35	2.12	1.62	1.63	2.88	2.45	2.54	
	CK-78-2 STN-07 FFG-13A	CK-78-2 STN-07 FFG-13B	CK-78-2 STN-07 FFG-14A	CK-78-2 STN-07 FFG-14B	CK-78-2 STN-08 FFG-15B	CK-78-2 STN-08 FFG-16	CK-78-2 STN-08 FFG-16	CK-78-2 STN-08 FFG-16	CK-78-2 STN-08 FFG-16	CK-78-2 STN-08 FFG-16	CK-78-2 STN-08 FFG-16	CK-78-2 STN-08 FFG-16	
Sample Type Description	Nodule B-2:20-31	Nodule B-5:~18-20	Nodule B-2:18-33	Nodule B~7:Un	Nodule B-11:20-13	Nodule B-11:20-13	Nodule B-11:20-13	Nodule B-11:20-13	Nodule B-11:20-13	Nodule B-11:20-13	Nodule B-11:20-13	Nodule B-11:20-13	Nodule B-14:10-20
Fe wt%	16.7	17.9	13.4	14.8	14.7								14.1
Mn	11.1	8.83	8.30	10.1	12.6								13.7
Fe/Mn	1.51	2.03	1.62	1.46	1.16								1.03
Si	12.5	13.8	16.8	14.6	11.6								11.2
Al	4.93	5.27	6.49	5.95	5.10								5.07
Mg	1.59	1.62	1.63	1.73	1.49								1.57
K	1.71	1.28	2.47	1.54	1.35								1.28
Ca	1.28	1.12	1.10	1.24	2.03								2.46
Na	1.54	1.52	1.48	1.55	2.06								2.06
P	0.27	0.25	0.18	0.23	0.32								0.47
Ti	1.35	1.33	0.86	1.02	1.64								1.52
LOI	22.0	21.9	20.5	23.2	20.1								23.7
H ₂ O ⁻	11.0	11.4	12.0	13.4	7.90								11.8
H ₂ O ⁺	7.50	7.00	6.40	7.20	9.90								7.9
Ag ppm	0.46	0.44	0.26	0.31	0.12								0.37
As	131	130	84	103	109								111
Ba	828	756	638	702	777								925
Be	3.3	3.4	2.3	2.7	3.3								3.2
Bi	7.5	7.4	5.1	6.1	5.7								6.3
Cd	3.7	2.7	2.8	3.4	5.2								6.2
Cl	5011	4628	3761	4342	4722								4660
Co	2742	2393	1705	2079	1933								1871
Cr	342	426	644	498	52								71
Cs	0.79	1.13	1.59	1.27	0.43								0.34
Cu	1663	1298	1580	1744	2465								3345
Ga	12	12	12	12	8.9								13
Hf	15	15	8.0	9.2	15								11
In	0.63	0.56	0.43	0.47	0.40								0.45
Li	58	52	76	73	88								103
Mo	146	103	116	133	132								137
Nb	92	89	51	60	88								79
Ni	2899	1986	2466	2806	2693								3776
Pb	742	743	442	562	592								586
Rb	32	39	49	41	20								26
S	1461	1242	1136	1270	1086								1701
Sb	33	32	21	26	32								33
Sc	22	28	30	27	11								14
Se	1.0	0.68	0.68	0.58	0.76								0.68
Sn	5.2	5.9	3.0	3.7	16								6.6
Sr	681	633	466	567	708								823
Ta	2.0	2.1	1.1	1.4	2.4								2.1
Te	15	14	11	13	10								8.6
Th	44	48	20	27	22								22
Tl	75	55	63	73	98								113
U	6.7	6.3	4.5	5.8	7.7								7.0
V	425	391	281	323	358								385

(continued on next page)

Table A.1 (continued)

Sample Type Description	CK-78-2 STN-07 FFG-13A Nodule B-2:20-31	CK-78-2 STN-07 FFG-13B Nodule B-5:~18-20	CK-78-2 STN-07 FFG-14A Nodule B-2:18-33	CK-78-2 STN-7 FFG-14B Nodule B~7:Un	CK-78-2 STN-08 FFG-15B Nodule B-11:20-13	CK-78-2 STN-08 FFG-16 Nodule B-14:10-20		
W	28	20	20	24	24	26		
Zn	447	432	380	433	423	552		
Zr	578	565	352	433	516	524		
Hg ppb	–	–	–	–	64	–		
Au	–	–	–	–	–	–		
Ir	–	–	–	–	–	–		
Os	–	–	–	–	–	–		
Pd	–	–	–	–	–	–		
Pt	–	–	–	–	–	–		
Rh	–	–	–	–	–	–		
Ru	–	–	–	–	–	–		
La ppm	144	126	87.8	109	127	133		
Ce	803	764	431	547	420	421		
Pr	35.3	32.1	20.9	26.4	30.3	32.7		
Nd	130	117	79.3	100	125	125		
Sm	29.6	26.3	17.5	23.0	27.5	27.7		
Eu	6.82	6.46	4.06	5.25	6.92	6.75		
Gd	29.8	26.4	18.0	22.6	30.5	29.4		
Tb	4.70	4.11	2.90	3.64	4.86	4.64		
Dy	28.1	24.2	17.4	22.2	29.3	29.0		
Y	104	85.3	68.6	83.6	124	128		
Ho	5.46	4.79	3.47	4.35	5.92	5.96		
Er	15.2	12.5	9.27	11.5	16.6	15.9		
Tm	2.17	1.83	1.39	1.73	2.58	2.43		
Yb	14.5	11.9	8.86	11.3	16.5	16.6		
Lu	2.19	1.92	1.42	1.84	2.38	2.46		
Σ REY ¹	1356	1246	772	974	969	979		
%Heavy ²	15.7	14.4	17.5	17.2	24.7	24.6		
Ce _{cn} ³	2.65	2.83	2.35	2.39	1.59	1.50		
Ce _{sn} ³	2.60	2.77	2.32	2.35	1.56	1.47		
Sample Type Description	CK-80-1 STN-03 WGCM-03	CK-80-1 STN-03 WGCM-13	CK-80-1 STN-04 WGCM-04A	CK-80-1 STN-04 WGCM-04B	CK-80-1 STN-10 WGCM-08	CK-80-2 STN-17 WG-01A	CK-80-2 STN-17 WG-01B-MRT-B0-8	CK-80-2 STN-17 WG-01B-MRU-B0-11
Fe wt%	17.0	15.8	11.4	12.7	10.6	13.8	14.3	16.2
Mn	19.9	18.7	21.7	19.2	16.2	17.7	17.4	18.8
Fe/Mn	0.85	0.85	0.52	0.66	0.65	0.78	0.82	0.86
Si	7.10	6.77	7.89	9.68	12.9	7.71	7.39	7.58
Al	3.06	2.94	4.20	4.24	4.74	3.67	2.95	2.94
Mg	1.24	1.22	2.09	1.73	1.85	1.36	1.14	1.22
K	0.83	0.80	1.18	1.26	1.73	0.84	0.77	0.85
Ca	2.74	1.86	1.71	1.73	1.45	1.87	1.96	1.96
Na	1.92	1.79	2.12	2.13	2.37	1.79	1.80	1.91
P	0.33	0.30	0.29	0.29	0.21	0.28	0.28	0.31
Ti	1.05	0.99	0.77	0.81	0.82	0.94	0.91	0.95
LOI	33.0	26.4	28.3	29.2	25.1	26.9	29.2	24.5
H ₂ O ⁻	21.0	8.20	15.9	17.9	13.9	7.80	7.60	8.70
H ₂ O ⁺	7.40	13.7	7.90	7.00	7.10	15.3	17.3	12.2
Ag ppm	0.38	0.09	0.23	0.21	0.21	0.09	0.12	0.05
As	166	155	124	133	101	126	134	153
Ba	1380	1176	1189	1158	947	1011	1169	1391
Be	4.9	4.2	2.9	3.5	2.8	3.9	4.7	4.9
Bi	13	13	8.0	9.6	6.8	11	10	13
Cd	4.4	4.6	9.7	6.8	6.8	5.7	4.1	3.4
Cl	7772	6740	7004	7296	6039	6106	6795	7410
Co	3962	3943	2699	2801	2056	3623	3766	4009
Cr	11	1.1	14	19	29	5.4	8.7	19
Cs	<0.1	0.22	0.24	0.37	0.46	0.22	0.32	0.33
Cu	2506	2342	5482	3666	4065	2527	2078	1774
Ga	11	3.9	20	18	21	5.5	5.1	3.8
Hf	13	15	9.5	9.7	9.3	12	11	13
In	0.95	0.84	0.45	0.57	0.48	0.74	0.75	1.10
Li	32	35	168	91	85	57	32	27
Mo	385	414	422	395	308	330	356	398
Nb	87	87	65	69	56	74	63	82
Ni	3962	3214	8609	6577	6725	3449	2749	2705
Pb	999	1046	684	716	515	893	882	1023

Table A.1 (continued)

Sample Type Description	CK-80-1 STN-03 WGCM-03 Nodule B-2:~28-30	CK-80-1 STN-03 WGCM-13 Nodule B-3:~33-15	CK-80-1 STN-04 WGCM-04A Nodule B-5:12-23	CK-80-1 STN-04 WGCM-04B Nodule B-9:~8-20	CK-80-1 STN-10 WGCM-08 Nodule B-1:48	CK-80-2 STN-17 WG-01A Nodule B-2:32-~20	CK-80-2 STN-17 WG-01B-MRT-B0-8 PC Nod B:8	CK-80-2 STN-17 WG-01B-MRU-B0-11 PC Nod B:11	
Rb	14	12	19	21	29	13	11	12	
S	2532	1852	1902	1949	1510	1735	1840	2191	
Sb	38	35	39	38	31	34	29	31	
Sc	12	8.2	11	13	16	7.6	6.9	7.7	
Se	0.89	0.87	0.83	0.97	0.70	0.76	0.65	0.55	
Sn	6.7	9.4	4.3	5.4	6.9	5.9	5.5	7.4	
Sr	1081	991	818	865	708	854	1005	1117	
Ta	1.7	1.7	1.1	1.4	1.3	1.5	1.8	1.6	
Te	27	25	12	17	10	22	27	31	
Th	29	29	16	18	17	26	27	29	
Tl	165	178	164	141	142	180	162	172	
U	9.9	11	6.9	6.7	5.5	9.3	9.7	11	
V	558	526	460	459	367	407	442	515	
W	71	73	76	68	48	55	60	83	
Zn	486	420	698	566	515	479	437	440	
Zr	624	578	490	505	423	482	403	558	
Hg ppb	–	9	–	–	–	12	13	11	
Au	6	3	–	–	7	–	4	–	
Ir	6	6	–	–	2	–	5	–	
Os	3	–	–	–	–	–	–	–	
Pd	9	3	–	–	10	–	5	–	
Pt	237	224	–	–	141	–	180	–	
Rh	18	17	–	–	8	–	15	–	
Ru	20	19	–	–	12	–	17	–	
La ppm	196	182	140	146	118	139	155	192	
Ce	1061	979	554	719	521	850	948	1271	
Pr	45.3	41.3	33.1	34.6	28.2	31.0	35.9	45.2	
Nd	166	166	126	128	105	127	145	183	
Sm	37.0	36.8	28.9	28.3	23.9	27.4	31.9	40.0	
Eu	8.56	8.99	6.58	6.39	5.80	6.84	7.81	9.78	
Gd	38.0	38.7	28.8	29.7	24.0	30.0	33.1	41.7	
Tb	6.11	6.27	4.72	4.76	3.88	4.90	5.50	6.78	
Dy	38.2	37.8	28.9	29.5	22.9	29.4	32.4	39.9	
Y	147	144	132	128	93.4	124	121	146	
Ho	7.53	7.86	6.18	5.97	4.75	6.01	6.76	8.30	
Er	20.8	21.6	16.5	16.6	13.0	17.0	18.3	22.6	
Tm	3.39	3.43	2.54	2.53	1.99	2.70	2.78	3.47	
Yb	21.5	22.5	16.9	16.9	12.9	17.9	18.2	22.6	
Lu	3.38	3.16	2.68	2.73	2.10	2.53	2.62	3.24	
Σ REY ¹	1799	1699	1128	1299	982	1415	1564	2034	
%Heavy ²	16.4	17.3	21.8	18.7	18.8	17.0	15.9	14.9	
Ce _{cn} ³	2.63	2.63	1.90	2.36	2.11	3.01	2.97	3.19	
Ce _{sn} ³	2.60	2.61	1.88	2.33	2.08	2.99	2.93	3.15	
Sample Type Description	1021-G991 Nodule B-1:28	1021-G995 Nodule B-1:31	1021-G1001 Nodule B-1:42	1021-G1003 Nodule B-1:32	1021-G1004 Nodule B-1:38	U321A Nodule B-1:30	U339<20mm Nodule B-4:15-19	U339>20mm Nodule B-1:30	U340 Nodule B-1:37
Fe wt%	19.0	16.3	16.3	15.2	13.7	13.1	17.4	16.5	13.6
Mn	13.8	14.7	8.18	15.5	18.7	16.3	17.0	15.7	14.5
Fe/Mn	1.38	1.11	1.99	0.98	0.73	0.80	1.02	1.05	0.94
Si	7.45	6.36	11.3	6.86	6.17	8.77	7.01	6.96	11.3
Al	3.57	2.92	3.62	3.21	3.10	3.88	2.65	2.48	4.53
Mg	1.21	1.25	2.23	1.29	1.43	1.45	1.35	1.18	1.35
K	0.73	0.62	0.97	0.66	0.59	1.18	0.80	0.92	1.73
Ca	1.52	1.80	3.46	1.72	1.94	1.90	2.64	2.04	2.01
Na	1.24	1.14	1.51	1.21	1.27	1.95	1.79	1.77	2.29
P	0.34	0.34	0.32	0.32	0.31	0.35	0.53	0.37	0.39
Ti	1.32	1.28	2.11	1.10	1.00	0.90	1.44	1.37	1.04
LOI	27.5	31.4	23.0	33.4	30.5	26.4	25.2	29.9	23.1
H ₂ O ⁻	10.3	8.90	7.50	10.0	9.90	8.30	8.60	8.70	9.70
H ₂ O ⁺	16.3	20.6	12.5	19.9	17.6	13.7	12.3	17.5	10.1
Ag ppm	–	–	–	–	–	0.16	0.20	0.18	0.17
As	191	178	126	173	166	128	146	150	125
Ba	971	1008	701	996	1110	1073	1225	1117	947
Be	5.6	5.4	3.2	5.0	5.0	3.6	4.3	4.3	3.2
Bi	13	14	7.1	12	12	7.8	11	10	6.9
Cd	4.8	4.4	1.6	5.1	6.7	5.2	3.6	2.9	4.3
Cl	5753	5280	12865	5822	5727	5850	7718	6697	5787

(continued on next page)

Table A.1 (continued)

Sample Type Description	1021-G991 B-1:28	1021-G995 Nodule B-1:31	1021-G1001 Nodule B-1:42	1021-G1003 Nodule B-1:32	1021-G1004 Nodule B-1:38	U321A Nodule B-1:30	U339<20mm Nodule B-4:15-19	U339>20mm Nodule B-1:30	U340 Nodule B-1:37
Co	3489	4391	3395	4533	4528	2694	4267	4140	2326
Cr	17	24	144	16	13	24	60	37	28
Cs	0.56	0.66	0.54	0.56	0.44	0.22	0.22	0.33	0.33
Cu	1672	1570	436	1778	2220	2683	1849	1588	2237
Ga	19	18	17	20	24	5.9	<0.1	0.11	5.3
Hf	–	–	–	–	–	9.8	14	12	10
In	1.1	0.92	0.39	0.84	0.78	0.56	0.75	0.71	0.45
Li	51	37	16	51	78	68	22	13	50
Mo	213	239	102	277	340	322	232	256	268
Nb	108	120	108	107	82	71	85	74	76
Ni	2832	3282	1066	4078	4795	4329	3304	2694	3488
Pb	992	1041	638	949	968	735	897	826	703
Rb	13	12	17	13	10	18	12	14	26
S	1003	1207	1405	1222	1221	1636	2079	1972	1550
Sb	34	35	27	36	34	30	34	34	29
Sc	16	15	19	16	13	11	11	10	11
Se	0.78	0.77	0.65	0.67	0.44	0.76	0.66	0.99	0.89
Sn	7.1	6.9	8.0	6.2	6.1	5.6	9.1	7.6	5.3
Sr	769	804	836	774	860	833	1073	1084	803
Ta	2.0	2.4	4.8	1.9	1.3	1.5	1.9	2.3	1.7
Te	15	23	16	27	24	17	29	27	16
Th	70	43	39	45	39	21	24	24	25
Tl	97	137	42	133	189	158	154	133	122
U	8.5	8.7	6.2	8.1	7.8	8.2	10	11	8.1
V	531	523	390	520	493	414	457	447	405
W	40	48	21	54	67	56	50	49	44
Zn	650	625	546	604	484	484	473	433	416
Zr	–	–	–	–	–	531	616	553	540
Hg ppb	22	72	8	22	16	5	<5	<5	11
Au	–	–	–	–	–	–	–	–	–
Ir	–	–	–	–	–	–	–	–	–
Os	–	–	–	–	–	–	–	–	–
Pd	–	–	–	–	–	–	–	–	–
Pt	–	–	–	–	–	–	–	–	–
Rh	–	–	–	–	–	–	–	–	–
Ru	–	–	–	–	–	–	–	–	–
La ppm	173	186	148	177	153	169	209	204	159
Ce	1215	1120	728	1167	1032	739	993	1001	660
Pr	45.9	46.3	35.7	44.1	38.0	35.9	43.8	44.7	36.8
Nd	172	172	133	163	141	146	175	181	148
Sm	40.5	39.7	29.2	37.1	32.1	33.7	38.8	38.9	35.7
Eu	9.69	9.31	7.32	8.96	7.84	8.47	9.61	9.97	8.52
Gd	39.4	37.5	28.0	36.6	31.5	37.6	42.8	42.6	36.5
Tb	7.05	6.53	4.61	6.46	5.48	6.12	6.65	6.70	6.08
Dy	38.0	36.1	25.2	34.9	30.2	36.3	38.0	37.3	35.5
Y	149	147	105	152	130	171	154	142	159
Ho	8.16	7.84	5.31	7.72	6.69	7.50	7.74	7.68	7.23
Er	21.1	20.5	13.5	19.9	17.6	21.2	22.5	21.9	20.4
Tm	3.36	3.26	2.06	3.24	2.80	3.08	3.38	3.13	2.93
Yb	21.2	20.4	12.8	20.2	17.6	20.2	21.1	20.4	18.9
Lu	3.32	3.26	1.94	3.20	2.76	3.18	3.33	3.21	2.89
ΣREY ¹	1947	1855	1280	1881	1649	1439	1769	1764	1339
%Heavy ²	15.4	15.7	16.1	15.6	15.3	21.9	17.5	16.7	22.3
Ce _{cn} ³	3.23	2.84	2.35	3.11	3.18	2.19	2.39	2.43	2.01
Ce _{sn} ³	3.14	2.78	2.31	3.05	3.12	2.19	2.39	2.42	1.99

¹ ΣREY = sum of rare earth elements plus yttrium.² Percentage of the REY complement that are heavy REY (Eu through Lu + Y).³ Ce_{cn} is Ce anomaly normalized to chondrite values; Ce_{sn} is Ce anomaly normalized to PAAS values.

⁴ B is bulk, L is layer; first number is number of nodules analyzed and the second and third numbers are maximum diameter of nodule or range of maximum diameter of nodules; Un is unknown because nodules were fragmented; PC Nod is pancake nodule; MRT is the most recent top and MRU is most recent underside for pancake nodules.